Diamond & Related Materials 161 (2026) 113095

Contents lists available at ScienceDirect

Diamond & Related Materials

journal homepage: www.elsevier.com/locate/diamond

Exploring the interaction of pristine and hybrid nanocages with 5-fluorouracil

Mohammad A. Matin [a,*], Md. Alauddin [b], Tapas Debnath [b], Abu Asaduzzaman [c], Joonkyung Jang [d]

[a] Computing Research Laboratory, Centre for Advanced Research in Sciences (CARS), Dhaka University, Dhaka, 1000, Bangladesh
[b] Department of Theoretical and Computational Chemistry, Dhaka University, Dhaka, 1000, Bangladesh
[c] Department of Chemistry, School of Science, Engineering and Technology, Pennsylvania State University – Harrisburg, Middletown, PA, 17057, USA
[d] Department of Nanoenergy Engineering, Pusan National University, Busan, 46241, Republic of Korea

ARTICLE INFO

Keywords:
5-Fluorouracil
$B_6C_6N_{12}$ nanocage
Drug delivery
Hetero-nanocages
Density functional theory

ABSTRACT

Advancements in nanoscience have accelerated the development of nanomaterials as carriers for anticancer drug delivery and sensors in clinical applications. Using Density Functional Theory (DFT) at the B3LYP-GD3(BJ)/6-31G(d,p) level, this study evaluated the adsorption efficiency of pristine C_{24} and $B_{12}N_{12}$ nanocages alongside hybrid nanocages ($B_{12}C_6N_6$, $B_6C_6N_{12}$, and $C_{12}B_6N_6$) for the anticancer drug 5-fluorouracil (5-FU). Adsorption energies ranged from −4.15 to −34.87 kcal mol^{-1}, with hybrids exhibiting stronger binding than pristine cages. Thermodynamic parameters confirmed spontaneous and exothermic adsorption, with Gibbs free energy changes (ΔG) reaching as low as -21.89 kcal mol^{-1} at 298 K. Modifying pristine nanocages into hybrids altered geometry, increased dipole moments by up to 253 %, reduced energy gaps by 73.22 % ($B_{12}C_6N_6$) and 71.47 % ($B_6C_6N_{12}$), and enhanced reactivity. While pristine C_{24} and $B_{12}N_{12}$ showed minimal sensitivity to 5-FU, hybrids $C_{12}B_6N_6$ and $B_6C_6N_{12}$ demonstrated significantly higher electronic sensitivities (ΔE_g = 31.31 % and 64.29 %), exceeding previous reports. $B_6C_6N_{12}$ exhibited the strongest adsorption, forming a stable conjugated complex ideal for drug delivery and detection in gas and solvent phases. Frontier molecular orbital (FMO), natural bond orbital (NBO), and non-covalent interaction (NCI) analyses confirmed significant charge transfer (~ − 0.31e) and dominant van der Waals interactions. UV–Vis and ADMP molecular dynamics simulations validated 5-FU binding stability, revealing minimal structural fluctuations over 1000 fs in aqueous environments. These quantitative findings highlight $B_{12}N_{12}$-based hybrids as promising smart carriers for 5-FU, encouraging further theoretical and experimental development of advanced drug delivery systems.

1. Introduction

Cancer is a significant group of diseases that can originate in any organ or tissue due to the uncontrolled growth of abnormal cells [1]. These cells can invade nearby body parts and spread to other organs, a process called metastasis, which is the leading cause of cancer-related deaths. Other common terms for cancer include neoplasia or malignant tumor. Cancer is a significant global health issue and the second leading cause of death, responsible for around 9.6 million deaths in 2018, or one in six deaths [2]. However, many cancers can be effectively treated through surgery, radiation, or chemotherapy, especially when detected early [3]. However, the effectiveness of anticancer drugs is limited by their low selectivity for cancer cells and poor water solubility [4,5]. Furthermore, anticancer drugs can lead to side effects on healthy tissues and organs [6,7]. 5-Fluorouracil (5-FU) is a heterocyclic compound widely used to treat head, neck [8], colon, and breast cancers [9]. Its structure resembles the pyrimidine molecules found in DNA and RNA, allowing 5-FU to interfere with nucleoside metabolism and integrate into RNA and DNA, leading to cytotoxicity and cell death [10]. However, despite its anticancer efficacy, 5-FU can cause severe side effects, including myelotoxicity, hand-foot syndrome, stomatitis, neurotoxicity, chest pain, cardiotoxicity, low blood counts, and cognitive impairment, which limit its clinical use [11]. This highlights the urgent need for the development of nanocarriers that can reduce these side effects while preserving the drug's pharmacophoric properties.

In recent years, nanomaterials have gained significant attention as

* Corresponding author.
E-mail address: matin123@du.ac.bd (M.A. Matin).

https://doi.org/10.1016/j.diamond.2025.113095
Received 13 August 2025; Received in revised form 3 November 2025; Accepted 15 November 2025
Available online 17 November 2025

carriers for the 5-FU anticancer drug. To address the toxicity of anticancer drugs, the scientific community has developed various strategies, with one of the most popular being the design of drug delivery nanovehicles [12]. Nanomaterial-based delivery systems are significantly impacting cancer immunotherapy due to their unique biological properties. Their high surface area to volume ratio, small size, and ability to bind or adsorb anticancer agents make them highly effective. Among various nanostructures such as nanodots, nanosheets, nanocages, nanowires, nanocones, and nanotubes, nanocages stand out for their spherical shape, reduced side effects, and increased sensitivity to drug molecules, attracting substantial research interest [13,14]. Among established drug carriers, fullerene-based nanomaterials stand out due to their feasible synthesis and versatile structures [15–20]. Specifically, heteronuclear fullerene-like structures, particularly group III nitrides, have shown immense potential in drug design, chemical sensors, and nanoelectronic devices, attributed to their exceptional stability and impressive chemical and physical properties [21,22].

The physical, chemical, thermal, and electronic properties of carbon and boron nitride fullerene-like nanostructures have attracted significant academic interest, emphasizing the need for detailed assessments to explore their potential applications [23,24]. These nanomaterials have demonstrated considerable potential in various applications, including drug delivery [25], energy storage [26], ion storage [27], catalysis [28], gas sensing [29], and optoelectronics [30]. Several studies have explored the potential of C_{24} fullerene for sensing and encapsulating various pharmaceuticals, demonstrating its effectiveness in drug delivery and sensing applications [31,32]. Inorganic boron nitride ($B_{12}N_{12}$) fullerene attracted interest after its synthesis through the arc-melting method and analysis using LD-TOF mass spectrometry [33]. $B_{12}N_{12}$ nanocages are isoelectronic with carbon nanocages but differ due to the ionic interactions between boron and nitrogen atoms [23,34]. Chukwuemeka et al. proposed that $B_{12}N_{12}$ decorated with transition metals could be a favorable carrier for 5-FU based on Density Functional Theory (DFT) studies [35]. Soltani et al. studied the interaction of 5-aminovaleric acid (5-AVA) drug molecules with $B_{12}N_{12}$ and $B_{16}N_{16}$ nanocages, concluding that $B_{12}N_{12}$ exhibited better suitability for drug delivery [36]. Fatemeh Azarakhshi et al. studied the adsorption of sulfanilamide on $B_{12}N_{12}$ and $Al_{12}N_{12}$ using DFT, concluding that $B_{12}N_{12}$ is suitable for sulfanilamide delivery [37]. Padash et al. found that $Al_{12}N_{12}$ had the best adsorption properties among $Al_{12}N_{12}$, $Al_{12}P_{12}$, $B_{12}N_{12}$, and $B_{12}P_{12}$ for sulfamide drugs [38]. Cytotoxicity is a crucial factor in developing nanomaterial-based drug delivery systems, as it directly impacts their biological applications. Recent studies indicate favorable outcomes for the cytotoxicity and biocompatibility of carbon and boron nitride (BN) nanostructures [39,40]. Vishwakarma et al. have conducted theoretical studies on how C_{24} nanocages interact with different drugs [41]. Hosseinian et al. found that 5-FU had limited interaction with pure C_{24} fullerene, but replacing a carbon atom with boron greatly enhanced adsorption [42]. Guo et al. performed experimental and theoretical studies on boron nitride nanostructures and their substituted structures, demonstrating the potential for melphalan drug adsorption [43]. Furthermore, numerous studies have shown that $B_{12}N_{12}$ and its numerous modified structures have the ability to adsorb various drugs, including 5-FU [35,44], Sulfasalazine [45], Naproxen [46], Serine [47], Fluoroquinolone [48], Metformin [21], Chlormethane [49], Amphetamine [50], Flucytosine [51], Emodin [52], Azacitidine [53], Mercaptopyridine [54], Curcumin [55,56], Penicillamine [57], Favipiravir [58,59], Allopurinol [60], Hydroxyurea [61–63], Gemifloxacin [64], Ciprofloxacin [65], Isoniazid [66], 6-Thioguanine [67], Temozolomide [68], Procarbazine [69], Ifosfamide [23,25], Dacarbazine [70], Sulfasalazine [71], Carmustine [72], and Nitrosourea [73].

These outcomes suggest that these nanocage have potential for biomedical applications, including biosensing, bio-imaging, and targeted drug delivery. Recently, various hetero-nanocages have been investigated as promising drug delivery systems because of their distinctive properties, including strong interactions with drug molecules [74–76]. Muz et al. explored $C_{30}B_{15}N_{15}$ hetero-nanocages as carriers for favipiravir, while Hazrati et al. studied their potential for isoniazid delivery [75,77]. Theoretical studies by X. F. Fan et al. and Paul et al. confirmed that C_{12}–B_6N_6 and C_{12}–Al_6N_6 hetero-nanocages are energetically stable [76,78]. Studies have shown that $B_6C_6N_{12}$, $C_{12}B_6N_6$, and $C_{12}Al_6N_6$ hetero-nanocages are energetically stable [76,79]. Celaya et al. also explored the binding of melphalan to C_{24}-based hetero-nanocages, showing that substitution led to efficient adsorption [80]. Muktadir et al. illustrated that hetero-nanocages substituted with boron and aluminum exhibit an enhanced capacity to encapsulate the drug cisplatin [31].

The objective of this study is to identify materials with the most effective drug-carrying and sensing capabilities for the 5-FU drug, focusing on both pristine C_{24} and $B_{12}N_{12}$ nanocages, as well as their heteroatom-doped variants ($C_{12}B_6N_6$, $B_6C_6N_{12}$, and $B_{12}C_6N_6$). Initially, we assessed the interaction between C_{24} and 5-FU, which showed weak adsorption. To enhance this interaction, we substituted C atoms in the nanocages with B and N atoms. To investigate 5-FU bio-sensing, fullerene-like heteronanocages ($C_{12}B_6N_6$, $B_{12}C_6N_6$, and $B_6C_6N_{12}$) were designed as nano drug carriers aimed at reducing the side effects of 5-FU via carrier modification. By analyzing the geometric, electronic, adsorption, thermodynamics, desorption, release mechanism and stability of the drug, nanocages, and their conjugated systems, this study aims to identify a suitable adsorbent for 5-FU.We hope this study provides valuable insights into the drug delivery performance of heteroatom-doped $B_{12}N_{12}$ and its derivatives while also offering guidance for developing more efficient boron-based nanomaterials for antitumor drug delivery.

2. Computational methodology

This research extensively investigates the competence of pristine and heteroatom-doped nanocarriers for adsorbing 5-fluorouracil (5-FU). Density functional theory (DFT) calculations were conducted using the Gaussian 16 program [81]to examine the adsorption, responsiveness, and reactivity of pristine and hetero-nanocages toward 5-FU in gaseous and solvent phase. GaussView 6.0.16 was utilized for visualization purposes. The ground state optimizations of 5-FU, nanocages, and their complexes were performed using the Becke−3 − Lee − Yang−Parr (B3LYP) [82] exchange-correlation functional, combined with Grimme's third version of atomic pair-wise dispersion correction (D3) [83] and Becke−Johnson (BJ) damping (B3LYP-GD3(BJ)), was applied to account for long-range dispersion interactions during geometry optimization. In all cases, the geometries were optimized using Pople's6-31G(d,p) double-zeta split valence basis set and followed by a single-point energy calculation corrected for basis set superposition error (BSSE) using the same basis set [84]. Frequency calculations were also performed at the B3LYP-GD3(BJ)/6-31G(d,p) level to confirm that the optimized geometries correspond to true local minima on the potential energy surface. For solution-phase computations, the conductor-like polarizable continuum model (CPCM) [85]with water as the solvent was applied, using the same theoretical level as for gas-phase optimizations. After optimizing the geometry is gas phase, thermodynamic parameters, vibrational frequencies, charge transfer, molecular electrostatic potential (MEP), and time-dependent DFT (TD-DFT) analyses were conducted using the optimized geometries employed same theoretical method with 6–31 + G(d,p) basis set. The vibrational frequency analysis confirmed that the structures were at a local minimum on the potential energy surface [80]. The vibrational frequencies were scaled using a factor of 0.9627 [86]. All systems examined in this study were neutral (charge = 0 |e|) and stabilized in a singlet state (M = 2S + 1, with S representing the total spin). To determine the stability of the adsorbates and adsorbents, cohesive energy was calculated, as it is a key indicator of system stability. The cohesive energy of the drug and proposed adsorbent nanocages was determined using the following Eq.1 [29].

$$E_{Cohesive} = \frac{1}{Q}(E_T - bE_B - cE_C - nE_N - hE_H - oE_O - fE_F) \quad (1)$$

Here, E_T represents the total electronic energy of the drug or nanocages, while Q denotes the total number of atoms in the system. The total energies of isolated boron, carbon, hydrogen, nitrogen, fluorine, and oxygen atoms are denoted by E_B, E_C, E_N, E_H, E_O and E_F respectively, with b, c, n, h, o and f representing the quantity of each atom in the structure.

The adsorption energies, E_{ads} of 5-FU on the surfaces of the nanomaterials were determined using Eq. 2 [87].

$$E_{Ads} = E_{Complex} - E_{nanocage} - E_{5-FU} + E_{BSSE} \quad (2)$$

Here, $E_{Complex}$, $E_{nanocage}$, and $E_{5\text{-}FU}$ denote the total electronic energies of the combined complex, the nanocage adsorbent, and the 5-FU drug, respectively. E_{BSSE} denote the basis set superposition error energy.

The deformation energy following drug adsorption is calculated using Eq. 3 [88]:

$$E_{def} = E_{Drug/Nanocage\ in\ Conjugated\ Structure} - E_{Drug/Nanocage\ in\ Free\ \ State} \quad (3)$$

Where $E_{Drug/Nanocage\ in\ Conjugated\ Structure}$ and $E_{Drug/Nanocage\ in\ Free\ Sate}$ represents the total electronic energy of the drug or nanocage when it is in a bonded (interacting) structure and free or isolated(non-interacting) state.

The energy gap, E_g value is defined as Eq. 4;

$$E_g = E_{LUMO} - E_{HOMO} \quad (4)$$

The E_g value, representing the energy gap between the highest occupied molecular orbital (HOMO) and the lowest unoccupied molecular orbital (LUMO), is crucial for understanding electronic properties and reactivity.

To evaluate the electronic sensitivity (ΔE_g) of the interaction between 5-FU and nanocages, we investigated the E_g values of all species. The electronic sensitivity (ΔE_g) for the interaction was calculated as Eq. 5;

$$\Delta E_g = \left[\frac{\left(E_{gap(nanocage-5FU)} - E_{gap(nanocage)}\right)}{E_{gap(nanocage)}}\right] \times 100\% \quad (5)$$

Where $E_{gap(nanocage\text{-}5\text{-}FU)}$ represents the band gap of the interacting complexes, and $E_{gap(nanocage)}$ denotes the band gap of the nanocages.

Further, the charge transfer (Q_{CT}) due to the interaction between 5-FU and nanocages was calculated using the following equation:

$$Q_{CT} = Q_{(nanocage-5FU)} - Q_{(5FU)} \quad (6)$$

Here, $Q_{nanocage\text{-}5\text{-}FU}$ and $Q_{5\text{-}FU}$ denote the charges of the interacting complexes, and the isolated 5-FU drug molecule, respectively.

To evaluate the interaction between the drug and nanocages, and the stability of the interacting complexes, we calculated thermodynamic parameters at 298.15 K and 1 atm pressure [87]. GaussSum was utilized to produce the density of states (DOS), providing information about the electronic structures and orbital composition [89]. We used VMD software to illustrate the non-covalent interactions(NCI) of the drug-nanocage complexes [90]. Moreover, Multiwfn 3.7 software was used for reduced density gradient (RDG) analysis [91]. These methods provide detailed insights into charge distribution, orbital characteristics, and the nature of non-covalent interactions of drug-nanocage complexes. Atom Centered Density Matrix Propagation (ADMP) molecular dynamics simulations were employed to analyze the stability of 5-FU nanocages complexes.

3. Results and discussions

3.1. Geometrical and adsorption site analyses

The stable conformer of the 5-FU drug and nanocages (C_{24}, $B_{12}N_{12}$, $C_{12}B_6N_6$, $B_6C_6N_{12}$, $B_{12}C_6N_6$) was optimized at the ground state employing B3LYP-GD3(BJ)/6-31G(d,p) theory. Fig. 1 shows the most stable optimized geometries and the MEP for the nanostructures analyzed in this study. The 5-FU molecule, a heterocyclic aromatic organic compound, contains 12 atoms and resembles the pyrimidine structures found in DNA and RNA. The calculated length of the C4–F10 bond is 1.338 Å, which closely matches the experimental value of 1.348 Å as reported in previous studies [92]. Similarly, the calculated bond lengths for C1–O7 (1.216 Å) and C3–N2 (1.405 Å) are in good agreement with the experimental values of 1.233 Å and 1.408 Å, respectively [93,94]. Additionally, the observed atomic charges for O7, O9, and F10 in 5-FU are −0.566 e, −0.617 e, and − 0.311 e, respectively. The cohesive energy was found to be −6.33 eV per atom, citing its energetic stability. The neutral 5-FU molecule has a dipole moment of 3.89 Debye, consistent with the findings of Ogunwale et al. of 4.125 Debye [95]. This indicates an asymmetric charge distribution within the molecule. Furthermore, the calculated HOMO and LUMO energies of 5-FU are −6.79 eV and − 1.39 eV, respectively, resulting in an energy gap of 5.40 eV. These values are consistent with the findings of Wei-Ming Sun et al., who reported HOMO and LUMO energies of −6.97 eV and − 1.62 eV, with a gap of 5.35 eV [96].

The adsorbents under investigation for 5-FU adsorption consist of 24 atoms, arranged into six 4-membered rings and eight 6-membered rings. The C_{24} nanocage, with m3m (O_h) [31]symmetry, features C—C bond lengths of 1.50 Å in the 4-MRs and 1.38 Å in the 6-MRs. Previously reported bond lengths were 1.39 Å for the 4-MRs and 1.37 Å for the 6-MRs [53]. The $B_{12}N_{12}$ nanocage features a uniform arrangement of boron and nitrogen atoms and exhibits T_h symmetry [97,98], and B—N bond lengths of 1.48 Å in the 4-MRs and 1.44 Å in the 6-MRs. The bond lengths analyzed in this study align with those reported in previous works [31,97,99]. Both C_{24} and $B_{12}N_{12}$ nanocages exhibit zero dipole moments due to their uniform charge distribution, as confirmed by MEP analysis. The energy gaps for C_{24} and $B_{12}N_{12}$ are 2.55 eV and 6.87 eV, consequently, in agreement with earlier research [33,97]. The hetero-nanocage $C_{12}B_6N_6$ was formed by modifying the C_{24} nanocage, substituting 12 carbon atoms with six boron atoms and six nitrogen atoms. The $C_{12}B_6N_6$ hetero-cage contains two specific regions, one is the C_{12} site and the other is B_6N_6 site, and features four types of bonds: C—C, B—N, B—C and C—N, found in both 4-MRs and 6-MRs rings. The lowest-energy structure of the $C_{12}B_6N_6$ hetero-fullerene investigated here resembles those reported by Fan et al., which also lack of two other bonds B—B and N—N [76]. In the T_h symmetric $B_{12}N_{12}$ nanocage, six boron atoms were substituted with six carbon atoms to form the $B_6C_6N_{12}$ nanocage. The $B_6C_6N_{12}$ nanocage, identified as the most stable C1 symmetric structure, includes five distinct bond types: C—C,B-N, C—N, N—N, and B—C [80]. Six nitrogen atoms in the T_h symmetric $B_{12}N_{12}$ nanocage were replaced with carbon atoms to form the $B_{12}C_6N_6$ nanocage, as previously noted [80]. The studied isomer examined here includes two unique B—N and C—N types of sites. This is one of the most stable isomers among the 50 $B_{12}C_6N_6$ nanocage isomers, with parameters aligning with previous studies [31,76,79,80,100,101]. The cohesion energies (E_{coh}) of the studied complexes were calculated to evaluate their stable conformations. These energies, presented in Table 1 for all examined complexes in both gas and water phases, are notably negative, confirming the stability of the complexes. In this study, the calculated cohesive energy of $C_{12}B_6N_6$ is −6.92 eV, compared to the previously reported value of −7.673 eV [76].

According to electronegativity analysis (based on the negative value of chemical potential), the electronegativity values for carbon, boron and nitrogen are 2.55, 2.051 and 3.066, respectively [31]. As a result, the electronegativity difference for C_{24} is zero, while it is non-zero in other cases, suggesting an increase in ionic character after substitution. All adsorbents exhibit positive frequency modes that signify their stability, as evidenced by the analysis of IR vibrational frequencies presented in Table 2 (The smallest and largest values for the vibrational frequencies).

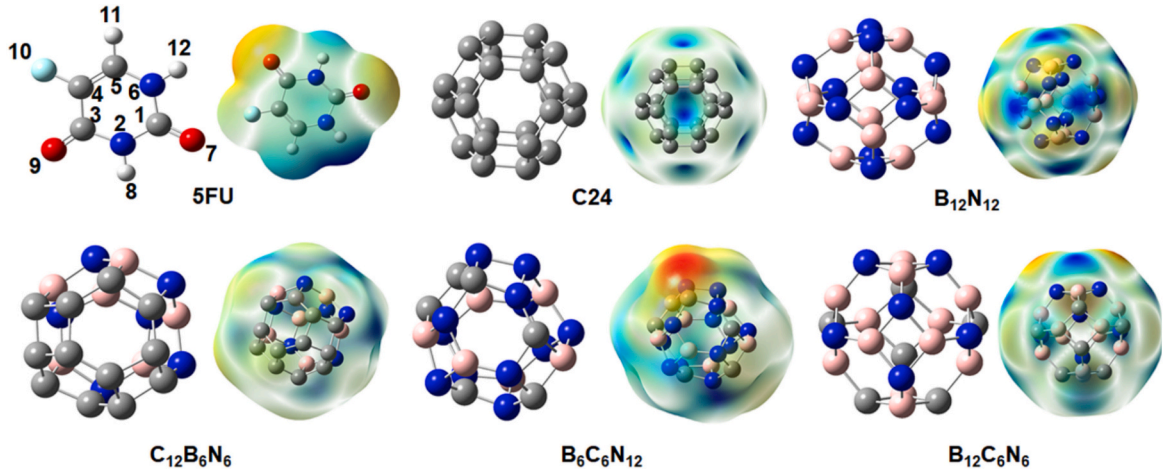

Fig. 1. The optimized Geometries and Molecular Electrostatic Potential (MEP) of 5-Flurouracil (5-FU) and nanocages.

Table 1
Adsorption Energy, E_{Ads} and Basis set superposition error energy, E_{BSSE} in kcal mol^{-1}; Deformation energies for drug and nanocages, $E_{def(Drug)}$ and $E_{def(Cage)}$ respectively in kcal mol^{-1}; Cohesive energy per atom, $E_{Cohesive}$ in eV and Nanocages-Drug contact distance (d) in angstroms (Å) at the gaseous phase.

Structure	State	E_{ads}	E_{BSSE}	$E_{def(Drug)}$	$E_{def\ (Cage)}$	$E_{Cohesive}$	d
5-FU						−6.33	
C_{24}						−8.10	
C_{24}@5FU	S1	−5.85	−3.99	0.05	0.09		3.26
C_{24}@5FU	S2	−6.54	−4.08	0.04	0.01		3.14
$B_{12}N_{12}$						−7.39	
$B_{12}N_{12}$@5FU	S_1	−28.82	−23.73	5.85	19.66		1.56
$B_{12}N_{12}$@5FU	S_2	−26.89	−21.95	4.70	18.79		1.56
$C_{12}B_6N_6$						−6.92	
$C_{12}B_6N_6$@5FU	S_1	−28.25	−25.42	6.95	19.18		1.56
$C_{12}B_6N_6$@5FU	S_2	−15.17	−23.65	3.16	13.33		1.63
$B_6C_6N_{12}$						−6.93	
$B_6C_6N_{12}$@5FU	S_1	−38.94	−33.49	10.00	20.56		1.52
$B_6C_6N_{12}$@5FU	S_2	−34.25	−27.33	5.97	21.19		1.50
$B_{12}C_6N_6$						−6.92	
$B_{12}C_6N_6$@5FU	S_1	−30.55	−23.10	6.11	20.22		1.56
$B_{12}C_6N_6$@5FU	S_2	−28.62	−9.33	4.92	19.37		1.63

Table 2
Thermodynamic parameters; enthalpy change, ΔH in kcal mol^{-1}; Gibbs Free energy change in kcal mol^{-1}, ΔG; entropy change, ΔS in kcal mol^{-1}. The smallest (ν_{sm}) and longest (ν_{lg}) peak location at vibrational frequency modes in cm^{-1} at gas phase.

Structure	State	ΔH	ΔG	ΔS	ν_{sm}	ν_{lg}
5-FU					112.11	3522.31
C_{24}					374.55	1556.19
C_{24}@5FU	S1	−4.15	5.40	−0.032	8.41	3479.77
C_{24}@5FU	S2	−5.51	2.55	−0.027	13.02	3521.10
$B_{12}N_{12}$					313.27	1398.49
$B_{12}N_{12}$@5FU	S_1	−19.03	−7.61	−0.038	16.84	3460.35
$B_{12}N_{12}$@5FU	S_2	−17.07	−5.69	−0.038	19.07	3499.95
$C_{12}B_6N_6$						
$C_{12}B_6N_6$@5FU	S_1	−31.35	−18.50	−0.043	19.47	3459.86
$C_{12}B_6N_6$@5FU	S_2	−0.37	−0.18	−0.001	20.56	3498.14
$B_6C_6N_{12}$						
$B_6C_6N_{12}$@5FU	S_1	−34.10	−20.91	−0.044	14.42	3497.21
$B_6C_6N_{12}$@5FU	S_2	−34.87	−21.89	−0.044	20.70	3501.59
$B_{12}C_6N_6$						
$B_{12}C_6N_6$@5FU	S_1	−28.25	−15.35	−0.043	19.31	3460.77
$B_{12}C_6N_6$@5FU	S_2	−22.34	−10.08	−0.041	12.32	3499.62

The interaction mechanism is crucial for a drug-carrier system. To determine whether $B_{12}N_{12}$ and its C, B, N-doped nanocages can serve as carriers for the 5-FU drug, geometry optimizations of C_{24} and its heteroatom-doped nanocages, along with the 5-FU drug, were carried out using the B3LYP-GD3(BJ)/6-31G(d,p) level of theory. Additionally, the interaction mechanism between 5-FU and these nanocages was explored by analyzing their active sites through MEP and Frontier molecular orbitals (FMO). MEP and FMO analyses can both qualitatively and quantitatively identify the electrophilic and nucleophilic regions in 5-FU and heteroatom-doped nanocages. MEP analysis shows(see Fig. 1) the electrostatic potential on the surface of the drug, where more positive areas indicate a higher likelihood of nucleophilic reactions, while more negative areas suggest electrophilic reactions. FMO analysis reveals the drug's active sites based on orbital energy. The HOMO is associated with electrophilic reactions as it tends to lose electrons, while the LUMO relates to nucleophilic reactions by accepting electrons. The results from Fig. 1 indicate that the oxygen (O) and fluorine (F) atoms of the 5-FU drug act as sites for electrophilic adsorption, while the other atoms participate in nucleophilic adsorption. The di-keto form is the most energetically stable tautomer of 5-FU [102]. The two carbonyl oxygen atoms represent the most negative regions, as illustrated by the MEP plot in Fig. 1. These oxygen atoms exhibit the strongest interaction with boron atoms, making this orientation the most stable configuration for adsorption [103]. For the C_{24} and its hetero-atom-doped nanocages, including $B_{12}N_{12}$, $B_{12}C_6N_6$, $C_{12}B_6N_6$, and $B_6C_6N_{12}$, the nucleophilic sites are the boron (B) atoms, except in the case of the C_{24} nanocage, where this is not applicable. The electrophilic sites are primarily the nitrogen (N) atoms. Therefore, it can be inferred that the 5-FU drug likely adsorbs to the B atoms of the nanocages via its O or F atoms, or interacts with the N atoms through its hydrogen (H) atoms. Several arrangements of the 5-

FU drug were analyzed to identify the minimum energy structure, leading to the determination of the most favorable configurations for 5-FU@$B_{12}N_{12}$ and its heteroatom-doped complexes (Fig. 2). Several initial configurations were tested, including parallel and perpendicular orientations, as well as different docking sites where functional groups of 5-FU could interact favorably with the nanocage surface. All configurations were optimized, and the most stable adsorption geometries were identified based on their adsorption energies and structural stability, as illustrated in Fig. S1. This approach ensures that the reported adsorption structures represent the most favorable and physically meaningful interactions between 5-FU and the nanocages.

In the evaluated structures, including S1 and S2 (Fig. 2), 5-FU interacts with the adsorbents mainly through the oxygen atom in the carbonyl group, located on the benzene ring opposite the fluorine atom or directly via the carbonyl oxygen.

3.2. Analysis of adsorption and thermodynamic properties

This research explores adsorption dynamics of the 5-FU drug on the prospective heteroatom-doped nanocages by evaluating adsorption energy and thermodynamic parameters, as shown in Tables 1 and 2, to identify the most effective adsorbents. The findings aim to determine the optimal nanocage for 5FU drug adsorption. Two distinct geometries, S1 and S2, were considered for each nanocage, based on alignment, adsorption energies, and thermodynamic stability (see Fig. 2). Figs. 1 and 2 demonstrate oxygen and fluorine atoms are highly susceptible to nucleophilic attack by the 5-FU drug due to their electron-rich nature. The basis set superposition error (BSSE) arises from artificial stabilization of a complex due to overlap of basis functions from interacting fragments. To ensure accurate adsorption energies, we applied the Boys–Bernardi counterpoise [104] correction to quantify and remove this error, providing reliable interaction energies. The most stable orientation of C_{24}@5FU exhibited an adsorption energy of −6.5 kcal mol^{-1}, which is corrected to −4.08 kcal mol^{-1} for basis set superposition error (BSSE). However, adsorption studies revealed that C_{24}'s adsorption capacity for the 5-FU molecule is inadequate. The $B_{12}N_{12}$ nanocage was designed to enhance adsorption by replacing the carbon atoms in C_{24} with boron and nitrogen. A naturally occurring pyrimidine nucleobase with oxo groups at positions 2 and 4 on the pyrimidine ring. The low-energy structures indicated that when the two nitrogen-containing hexagonal rings of 5-FU interact with the boron site on $B_{12}N_{12}$, a stable interaction energy of −28.82 kcal mol^{-1} (BSSE corrected to −23.73 kcal mol^{-1} in the S1 geometry with the original di-keto group) is achieved. This interaction is more stable than the one reported by Jaban et al. for 5-FU and boron nitride nanocage, highlighting the superior reactivity of $B_{12}N_{12}$ fullerenes compared to its other geometries [102]. Among the hetero-nanocages, the $B_6C_6N_{12}$ nanocage displays the most robust and suitable interactions with the 5-FU drug of S1 and S2 configurations. The interaction between the carbonyl oxygen site of 5-FU and the carbon/boron/nitrogen surface of $B_6C_6N_{12}$ results in the most favorable interaction. This study reveals a maximum adsorption energy of −38.94 kcal mol^{-1}(−33.49 kcal mol^{-1} BSSE corrected) for 5-FU interacting with the $B_6C_6N_{12}$ nanocage. In comparison, the $C_{12}B_6N_6$ and $B_{12}C_6N_6$ nanocages show maximum adsorption energies of −28.25 kcal mol^{-1}(−25.42 kcal mol^{-1} BSSE-corrected) and − 30.55 kcalmol^{-1} (−23.10 kcalmol^{-1} BSSE corrected), respectively. We have also calculated the adsorption energies (E_{ads}) employing several combinations of exchange–correlation functionals and basis sets: B3LYP-D3(BJ)/6-31G (d), B3LYP-D3(BJ)/6–311++G(d,p),M06-2×/6-31G(d,p), M06-2×/6–311++G(d,p), and ωB97XD/6–311++G(d,p). The comparative analysis showed consistent trends across all tested levels, with only minor variations in adsorption energies, confirming the robustness of our computational approach. The corresponding results are included in the Supporting Information (see Table S1).

Adsorption energies indicate that interactions can be classified as chemical or physical adsorption, depending on whether values exceed or fall below ±1 eV (±23 kcal mol^{-1}), [105] as shown in Table 1. Out of the five adsorbents, only the $B_6C_6N_{12}$ nanocage demonstrates substantial chemisorption in both configurations, indicating its superior adsorption capacity for 5-FU over the other nanocages.

Thermodynamic parameters, such as enthalpy change (ΔH), entropy change (ΔS), and Gibbs free energy change (ΔG), were determined 298.15 K and 1 atm. These calculations were conducted to explore the reaction mechanism 5-FU drug with the nanocages to evaluate the energy changes related to work and heat transfer. Analyzing these thermodynamic parameters provides insight into assessing if a reaction is endothermic (ΔH > 0) or exothermic (ΔH < 0). Additionally, changes in Gibbs free energy reveal whether the interaction is spontaneous (ΔG < 0) or non-spontaneous (ΔG > 0). The negative enthalpy changes confirm that the reaction between 5-FU and the nanocages is exothermic. Most reactions show negative ΔG values, indicating spontaneous interactions, except for the C_{24}@5FU conjugated structures, which display non-spontaneous behavior due to weak bonding. The decrease in entropy associated with the formation of bonded structures is advantageous, as shown in Table 2.

The moderate adsorption values indicate bond stability between the absorbed material and the substrate in the gas phase at room temperature. The confirmation that the 5-FU-adsorbed complexes attained an

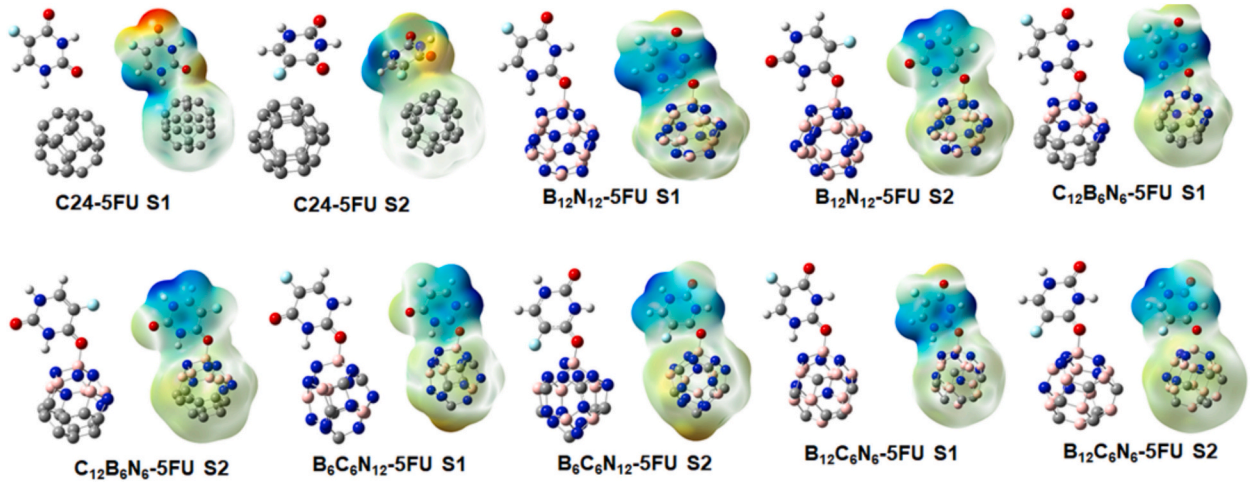

Fig. 2. Optimized geometries and molecular electrostatic potential (MEP) maps of conjugated complexes. The isovalue of 0.0004 electron/$Bohr^3$ is used to construct the MEP surfaces.

equilibrium point on the potential energy surface (PES) was based on the analysis of stability, vibrational infrared (IR) frequencies, and spectra (Fig. S5). After verifying the convergence criteria and positive frequency modes, it was determined that the conjugated geometries reached to minimum energy structure on the potential energy surface.

3.3. Analysis of electronic properties

The introduction of foreign atoms in triatomic hetero-nanocages disrupts uniform atomic distribution and generates dipole moments, demonstrating the effects of the substitution. This research explores the electronic characteristics of the systems by examining FMOs to assess their sensitivity, reactivity, electron distribution, and energy gaps. The calculated electronic parameters as presented in Table 3 and Figs. 3 and 4 illustrate the significant differences between the energy levels of the HOMO and LUMO.

Table 3 indicates that varying the proportions of carbon, boron, and nitrogen influences the energy levels of the HOMO and LUMO. These modifications also influence the energy difference between the HOMO and LUMO of the adsorbent nanocages. The calculated HOMO-LUMO gap, E_g of the nanocages C_{24}, $B_{12}N_{12}$, $C_{12}B_6N_6$, $B_6C_6N_{12}$, and $B_{12}C_6N_6$ were 2.55 eV, 6.87 eV, 3.13 eV, 1.96 eV, and 1.64 eV, respectively. These values are consistent with the previously reported calculations by Palash et al. [53] which listed values of 2.53 eV, 6.85 eV, 3.14 eV, 1.95 eV, and 1.83 eV. The $B_{12}N_{12}$ nanocage exhibits the highest HOMO energy level of −7.72 eV, whereas C_{24} shows a HOMO energy of −5.90 eV. Similarly, the LUMO energy of $B_{12}N_{12}$ is −0.85 eV, compared to −3.35 eV for C_{24}. Introducing C, B, and N atoms into the $B_{12}N_{12}$ nanocage leads to notable modifications in the HOMO-LUMO energy levels. In the $C_{12}B_6N_6$ nanocage, the HOMO energy decreases to −5.32 eV, while the LUMO energy increases to −2.48 eV, resulting in a narrowed HOMO-LUMO gap of 2.84 eV and a Fermi level shift to −3.90 eV. Similarly, in the $B_6C_6N_{12}$ nanocage, the HOMO energy drops to −4.97 eV, and the LUMO energy rises to −3.01 eV, reducing the HOMO-LUMO gap to 1.96 eV, with the Fermi level positioned at −3.90 eV. The observed changes in energy levels upon 5-FU adsorption on hybrid nanocage surfaces are primarily due to the stabilization of the LUMO and the destabilization of the HOMO. These shifts reflect electronic density redistribution and interactions between the adsorbate and the nanocage. For the $B_{12}C_6N_6$ nanocage, the HOMO energy decreases to −6.35 eV, while the LUMO energy increases to −4.51 eV, resulting in a narrowed energy gap of 1.84 eV and a Fermi level of −5.43 eV. The electronic properties of 5-FU interacting with nanocages and heteroatom-doped adsorbent complexes were analyzed in detail, focusing on the HOMO and LUMO as illustrated in Figs. 3 and 4. Significant alterations in the HOMO and LUMO energy levels were observed following drug adsorption onto the nanocages, as shown in Fig. 4. The reduction in HOMO energy lowered the ionization energy, enhancing electron mobility upon 5-FU adsorption. Initially, the HOMO and LUMO orbitals were evenly distributed across the drug molecule. After adsorption, however, the orbital distribution on the nanocage complexes became uneven as a result of charge transfer. Post-adsorption, the HOMO remained evenly distributed across the molecule, while the LUMO became predominantly localized on the 5-FU, with partial distribution shared between the adsorbent and the drug. Notably, the energy gap diminishes following the adsorption of the 5-FU molecule, as detailed in Table 3. The E_g energy gaps decreased after the adsorption of 5-FU on the nanocages, resulting in values of 2.46 eV, 4.56 eV, 2.84 eV, 1.57 eV, and 1.80 eV for the C_{24}@5FU, $B_{12}N_{12}$@5FU, $C_{12}B_6N_6$@5FU, $B_6C_6N_{12}$@5FU, and $B_{12}C_6N_6$@5FU complexes(S1 position), respectively. In particular, the energy gap of the conjugated structures decreases by as much as 43 % and 64 % for the $B_{12}N_{12}$ and $B_6C_6N_{12}$ nanocages, respectively, following 5-FU drug adsorption. In contrast, the adsorption of the azacitidine drug on these nanocages resulted in a decrease of 24.20 % and 42.70 %, respectively [53]. This reduction is the largest change in the energy difference noted in this study, emphasizing the impact of adsorption on the energy gap. A decrease in the E_g improves the responsiveness and conductivity of the nanostructures. The equation provided below illustrates the correlation between conductivity and variations resulting from substitution and the adsorption of the 5-FU drug [106].

$$\sigma = AT^{\frac{3}{2}}e^{\left(-E_g/2k_BT\right)} \tag{7}$$

Here, conductivity is denoted by σ, K_B represents Boltzmann's constant (2.0×10^{-3} kcal mol^{-1} K^{-1}), T is the temperature in Kelvin, and A is a constant with units of electrons m^{-3} K$^{-3/2}$. According to Eq. (7), the conductivity of the nanocages was calculated based on their energy gaps, and the results are summarized in Table S2. Nanocages such as $B_{12}N_{12}$, $B_6C_6N_{12}$, and $B_{12}C_6N_6$ exhibit tunable conductivity changes upon adsorption of drugs like 5-fluorouracil, enabling sensitive and selective detection. Among them, $B_6C_6N_{12}$ shows the highest conductivity. The magnitude of conductivity change correlates with the amount of adsorbed drug, providing a basis for real-time monitoring in biomedical applications. The systems analyzed in this study exhibit increased conductivity, especially after the substitution and adsorption of the drug. This suggests that changes in the energy gap are crucial for detecting 5-FU drug molecules with adsorbents, as they lead to the origination of an electrical signal.

3.4. Work function

Furthermore, when developing a drug-sensing device, it is important to take into account the Fermi level (E_F) and work function (Φ) of a

Table 3
HOMO energy, E_H in eV; LUMO energy, E_L in eV; energy gap, E_g in eV; change in energy gap, $\%\Delta E_g$; Fermi level energy, E_F, in eV, work function, Φ, in eV; Changes in work function, % Φ and Natural bond Orbital (NBO) charge transfer, from adsorbate to the adsorbent, Q_{NBO} in e unit at gas phase.

Structure	State	E_H	E_L	E_g	$\%\Delta E_g$	E_F	Φ	$\%\Phi$	Q_{NBO}
5-FU		−6.79	−1.39	5.40		−4.09	4.09		
C_{24}		−5.9	−3.35	2.55		−4.63	4.63		
C_{24}@5FU	S1	−6.04	−3.58	2.46	3.53	−4.81	4.81	4.00	0.004
C_{24}@5FU	S2	−5.79	−3.28	2.51	1.57	−4.54	4.54	1.95	−0.017
$B_{12}N_{12}$		−7.72	−0.85	6.87		−4.29	4.29		
$B_{12}N_{12}$@5FU	S_1	−6.94	−2.38	4.56	33.62	−4.66	4.66	8.75	−0.268
$B_{12}N_{12}$@5FU	S_2	−6.75	−2.84	3.91	43.09	−4.80	4.80	11.90	−0.272
$C_{12}B_6N_6$		−5.87	−2.74	3.13		−4.31	4.31		
$C_{12}B_6N_6$@5FU	S_1	−5.32	−2.48	2.84	9.27	−3.90	3.90	9.41	−0.276
$C_{12}B_6N_6$@5FU	S_2	−5.12	−2.97	2.15	31.31	−4.05	4.05	6.04	−0.279
$B_6C_6N_{12}$		−4.97	−3.01	1.96		−3.99	3.99		
$B_6C_6N_{12}$@5FU	S_1	−4.16	−2.59	1.57	19.90	−3.38	3.38	15.41	−0.268
$B_6C_6N_{12}$@5FU	S_2	−4.01	−3.31	0.70	64.29	−3.66	3.66	8.27	−0.169
$B_{12}C_6N_6$		−6.35	−4.51	1.84		−5.43	5.43		
$B_{12}C_6N_6$@5FU	S_1	−5.74	−3.94	1.80	2.17	−4.84	4.84	10.87	−0.258
$B_{12}C_6N_6$@5FU	S_2	−5.33	−3.54	1.79	2.72	−4.44	4.44	18.32	−0.308

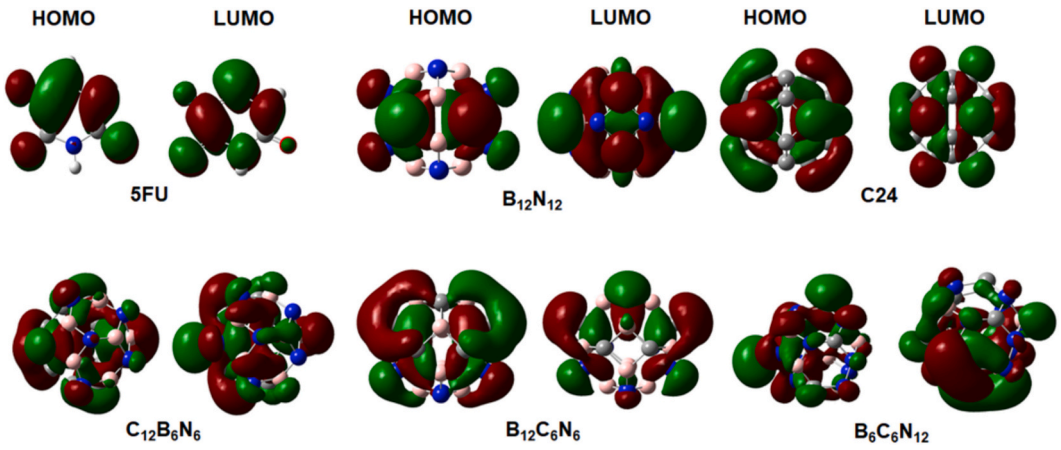

Fig. 3. Three–dimensional maps of the HOMO-LUMO electron distribution of 5-Flurouracil and nanocages with isovalue 0.02 a.u.

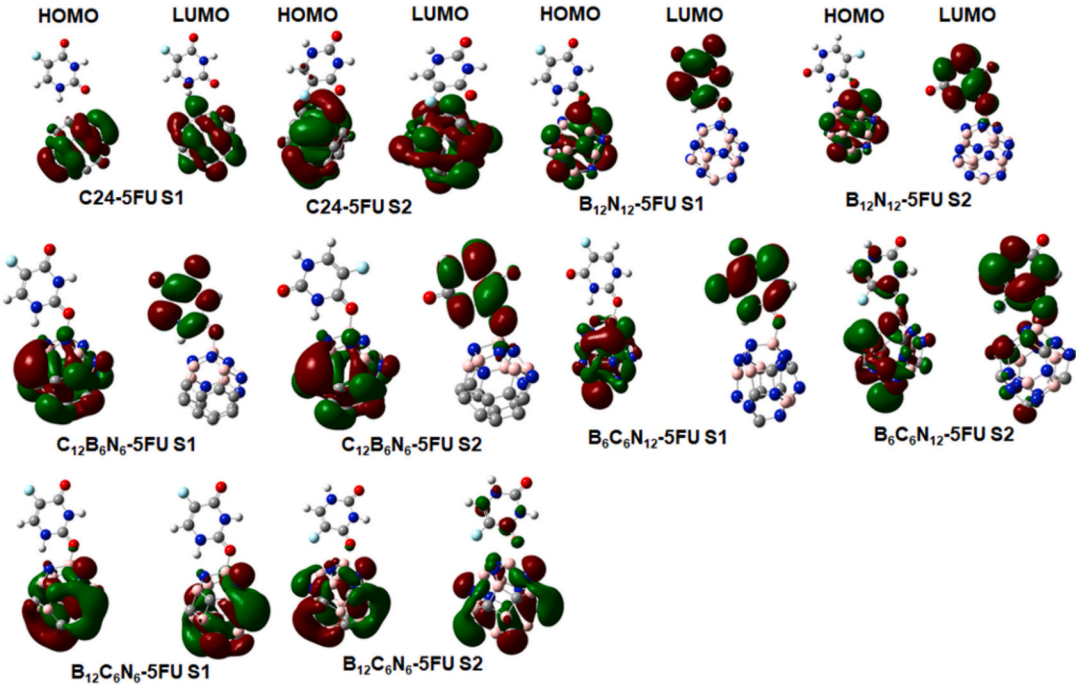

Fig. 4. Three–dimensional maps of the HOMO-LUMO electron distribution of the complexes with isovalue 0.02 a.u.

system. The work function represents the minimum energy required to remove an electron from the material's surface. The adsorption of 5-FU drug affects the energy gap of the material's surface, which in turn influences the work function. Variations in the work function can provide deeper insights into the responsive mechanism. The Fermi level and work function are related by the following equation [105,107,108].

$$\Phi = V_{el(+\infty)} - E_F \tag{8}$$

Here, the electrostatic potential of the material is indicated as $V_{el(+\infty)}$, which is considered be zero. Consequently, Eq. (8) simplifies to $\Phi = -E_F$, where E_F denotes the Fermi-level energy. Furthermore, Dushman's study suggested that fluctuations in the work function affect the surface current densities, subsequently altering the field emission properties. The Richardson-Dushman equation is utilized to examine the relationship with the work function and current density [106].

$$j = AT^2 e^{(-\Phi/k_B T)} \tag{9}$$

Here, A signifies the Richardson-Dushman constant, K_B refers to Boltzmann's constant, and T represents the temperature in Kelvin.

The current density of nanocages is highly sensitive to surface interactions, making it an important parameter for drug sensing. Adsorption of drugs such as 5-fluorouracil onto nanocages like $B_{12}N_{12}$, $B_6C_6N_{12}$, and $B_{12}C_6N_6$ alters the local electron distribution and electronic structure, leading to measurable changes in current density. These changes, directly linked to variations in electrical conductivity, serve as quantitative signals for drug detection. Using Eq. 9, the current densities of the adsorbed nanocages were calculated and are presented in Table S2. Among the studied systems, $B_6C_6N_{12}$ exhibits the highest current density, reflecting superior charge transport, sensing sensitivity, and faster response. The magnitude of the current density change correlates with the amount of adsorbed drug, enabling selective and real-time monitoring.

The adsorption of the 5-FU drug on various hybrid nanocages modifies the E_{HOMO} and E_{LUMO} energies, which in turn impact the work function (Φ). In this work, the computed Φ values and the corresponding variations in work function (ΔΦ) after adsorption are listed in Table 3.

The work function of hetero-nanocages notably diminishes following

the adsorption of 5-FU. Among them, the 5-FU–adsorbed $B_6C_6N_{12}$ nanocage displays the lowest work function, accompanied by a substantial change (ΔΦ) of 15.41 %. According to Eq. 9, as the work function decreases, the current density increases. This analysis indicates that developing a work function-based sensor utilizing these hetero-nanocages for 5-FU detection is practical.

3.5. Assessment of NBO, MEP, and charge transfer

Natural bond orbital (NBO) analysis clarifies the intra- and intermolecular interactions of filled and virtual orbitals, hybridization, and charge transfer arising from adsorbate-adsorbent interactions. NBO calculations employ the Fock matrix, a one-electron effective energy operator, to analyze NBO interaction energetics. The construction of bonding and antibonding natural orbitals between atoms x and y is mathematically represented through quantum mechanical equations that define these orbital interactions [97].

$$\Psi_{xy} = c_x\varphi_x + c_y\varphi_y \tag{10}$$

$$\Psi^{*}_{xy} = c_x\varphi_x + c_y\varphi_y \tag{11}$$

Where φ_x and $\varphi_y$are the atomic orbitals of atoms x and y accordingly, and $c_x$and$c_y$are coefficients that account for the contribution of each atomic orbital to the molecular orbital.

The localization degree of an atom is quantified by squaring the polarization coefficient, with larger values indicating higher electronegativity for that specific atom [97]. Moreover, the stability of molecules or complexes, which is influenced by electron delocalization, is directly related to the second-order perturbation energy $E^{(2)}$, commonly known as the stabilization energy [106]. This relationship helps to assess the strength of interactions within molecular systems and their overall stability.

$$E^{(2)} = q_i\frac{F_{ij}^2}{E_j - E_i} \tag{12}$$

In this equation, $q_i$represents the occupancy of the donor orbital, F_{ij} is the off-diagonal element of the NBO Fock matrix, and E_j and E_i denote the energies of the NBO orbitals. Supplementary Table S4 presents the calculations of key intermolecular NBO second-order interaction energies, as well as the occupancy rates and proportions of hybrid orbitals for both donor and acceptor. Intermolecular stabilization energies were reported solely for values exceeding 0.05 kcal mol. The Stabilization energy $E^{(2)}$ indicates the strength of donor(*i*)-acceptor(*j*) interactions arising from n → σ* or σ → σ* charge transfers. According to Table S4, for the C_{24}@5FU S1, the E^2 value is 1.71 kcal mol^{-1} for notable transitions include σ (C_1-C_{17}) → σ*(N_{31}-H_{36}). For $B_{12}N_{12}$@-5FU S1 complex, the E^2 value is 90.87 kcal mol^{-1} for LP (1) N_{31} → π*(2)C_{25}-O_{33}. The highest value of E^2 for $C_{12}B_6N_6$@-5FU S1 is 199.11 kcal mol^{-1} for LP(3) $O_{33(5FU)}$ → LP*(3)B_5 and for $B_6C_6N_{12}$@-5FU S1 199.05 kcal mol^{-1} for LP (1)C_1 → LP*(1)B_{21}. For the complex $B_{12}C_6N_6$@-5FU S1, the E^2 value is 301.08 kcalmol^{-1} for LP(1)N_{13} → BD*(2)B_4-O_{33}. The most significant intermolecular donor-acceptor transition observed in this study occurs in the $B_{12}C_6N_6$@-5FU S1 conjugated geometry, where the transition LP (1)N_{13} → BD*(2)B_4-O_{33} has a stabilization energy of 301.08 kcal mol^{-1}.

The charge difference among the natural bond orbitals of the 5-FU drug and the hetero-atom-doped nanocage was estimated using the Q_{NBO} parameter, as presented in Table 3. The NBO assessment illustrates that the uncharged 5-FU drug carries no overall charge. In contrast, in the bonded S2 geometry of $B_{12}C_6N_6$@5FU, the 5-FU drug displays a charge of +0.308 e, demonstrating its donor characteristics. Table 3 further indicates that in every complex structure, 5-FU serves as a donor while the nanocages function as charge acceptors. This analysis of charge transfer is supported by molecular electrostatic potential (MEP) maps, which depict regions of both high and low electron density. In the MEP illustrations, blue (Figs. 1 and 2) represents positive electrostatic potential, while yellow and red indicate negative electrostatic potential. The MEP maps reveal a stronger blue hue upon the 5-FU region in the bonded complexes as compared with the neutral molecule, suggesting that 5-FU becomes electropositive upon adsorption.

3.6. Dipole moment analysis and quantum molecular descriptors

As shown in Table 4, the dipole moment of the 5-FU molecule before adsorption is 3.89 Debye (D), highlighting its polar nature. Dipole moments were calculated for pure C_{24}, $B_{12}N_{12}$, and hetero-atom-doped nanocages $C_{12}B_6N_6$, $B_6C_6N_{12}$, and $B_{12}C_6N_6$, as well as their 5-FU nanocomplexes. The symmetrical structure of the pure C_{24} and $B_{12}N_{12}$ nanocages results in a dipole moment of zero. Introducing B, C, and N atoms into the $B_{12}N_{12}$ nanocage increases its dipole moment from zero to a range of 0.50 to 2.53 D. This increase is due to the disruption of charge symmetry caused by the presence of these heteroatoms. For 5-FU adsorbed onto heteroatom-doped $B_{12}N_{12}$ nanocages, the dipole moments range from 3.48 to 13.04 D. The observed change in dipole moment upon 5-FU adsorption results from charge transfer between the drug and the nanocages, causing a larger separation between the centers of positive and negative charges in the complex compared to the isolated system. As a result, the dipole moment of the complex increases. Furthermore, the increased dipole moment indicates that adsorption on the nanocage surface may improve the efficiency of drug transport within the body. The most pronounced change in dipole moment occurs when 5-FU is adsorbed onto the $B_6C_6N_{12}$ nanocage (13.04 D), while the C_{24}@5FU complex exhibits the smallest change in dipole moment (3.48 D). The incorporation of B, C, and N atoms to the system not only raises the dipole moment of the complex but also notably boosts the dipole moment of the drug molecules within it. This finding highlights the beneficial role of B, C, and N doping in promoting drug transport. The trend in dipole moment of 5-FU complexes follows the order: $B_6C_6N_{12}$@5FU > $B_{12}C_6N_6$@5FU > $C_{12}B_6N_6$@5FU > $B_{12}N_{12}$@5FU > C_{24}@5FU.

This study also analyzed various quantum molecular descriptors to improve comprehension of the stability and reactivity of the suggested complexes, as presented in Table 4. These parameters were derived using Eqs. 8–13 [58] based on extended Koopman's theorem, where the ionization potential (*I*) is related to the HOMO energy ($I = -E_H$), and the electron affinity (*A*) is related to the LUMO energy ($A = -E_L$) [97,109]. Table 4 reveals that the bonded systems demonstrate differences in chemical potential relative to naked systems, demonstrating considerable changes in thermodynamic states during the adsorption mechanism. Specifically, the hardness of the bonded systems typically diminishes, whereas their softness tends to increase compared to the bare drug and nanocage systems. Hardness measures the resistance of atoms, molecules or ions to deformation of their electron cloud, while softness is its reciprocal [31]. A decrease in hardness and an increase in softness typically suggest enhanced reactivity of the systems. This shift indicates that the conjugated systems are more reactive, which is a favorable characteristic in the context of adsorption and stability. Prior to adsorption, the global hardness values of the complexes were observed in the following increasing order: 0.92, 0.98, 1.28, 1.57 and 3.44 eV for $B_{12}C_6N_6$, $B_6C_6N_{12}$, C_{24}, $C_{12}B_6N_6$, and $B_{12}N_{12}$, respectively. Following 5-FU adsorption, these values shifted to 0.90, 0.79, 1.23, 1.42 and 2.28 eV for the same complexes, signifying enhanced reactivity and lower stability. Global softness values showed a close range between 0.146 and 0.543 eV shifted to 0.219 to 0.637 eV^{-1}.Increased values of chemical potential (μ) suggest enhanced reactivity and reduced stability. The electrophilicity index (ω) helps differentiate strong electrophiles from weak ones. The ranking of chemical potential was noted as $B_{12}C_6N_6$@5FU > C_{24}@5FU > $B_{12}N_{12}$@5FU > $C_{12}B_6N_6$@5FU > $B_6C_6N_{12}$@5FU, with corresponding values of −4.84, −4.81, −4.66, −3.90, and − 3.38 eV, respectively. Strong electrophilic characteristics were found in $B_{12}C_6N_6$@5FU (13.01 eV), C_{24}@5FU (9.40 eV), and $B_6C_6N_{12}$@5FU (7.26 eV). Analysis of E_g values are in both Tables 3 and 4

Table 4
Dipole moment, (μ_D) in Debye; The Energy Gap (E_g), Ionization Potential (*IP*), Electron Affinity (*EA*), Chemical Potential (μ), Electrophilic Index (ω), Chemical Hardness (η), Chemical Softness(*S*) and Electronegativity (χ) calculated for all systems. All units are electron volt (eV).

Systems	*state*	*D.M.*	E_g	*IP*	*EA*	μ	ω	η	*S*	χ
5-FU		3.89	5.40	6.79	1.39	−4.09	3.10	2.70	0.185	4.09
C_{24}		0.0	2.55	5.9	3.35	−4.63	8.39	1.28	0.392	4.63
C_{24}@5FU	S1	4.10	2.46	6.04	3.58	−4.81	9.40	1.23	0.407	4.81
C_{24}@5FU	S2	3.48	2.51	5.79	3.28	−4.54	8.19	1.26	0.398	4.54
$B_{12}N_{12}$		0.0	6.87	7.72	0.85	−4.29	2.67	3.44	0.146	4.29
$B_{12}N_{12}$@5FU	S_1	4.88	4.56	6.94	2.38	−4.66	4.76	2.28	0.219	4.66
$B_{12}N_{12}$@5FU	S_2	10.81	3.91	6.75	2.84	−4.80	5.88	1.96	0.256	4.80
$C_{12}B_6N_6$		0.50	3.13	5.87	2.74	−4.31	5.92	1.57	0.319	4.31
$C_{12}B_6N_6$@5FU	S_1	4.58	2.84	5.32	2.48	−3.90	5.36	1.42	0.352	3.90
$C_{12}B_6N_6$@5FU	S_2	11.72	2.15	5.12	2.97	−4.05	7.61	1.08	0.465	4.05
$B_6C_6N_{12}$		2.53	1.96	4.97	3.01	−3.99	8.12	0.98	0.510	3.99
$B_6C_6N_{12}$@5FU	S_1	13.04	1.57	4.16	2.59	−3.38	7.26	0.79	0.637	3.38
$B_6C_6N_{12}$@5FU	S_2	11.71	0.70	4.01	3.31	−3.66	19.14	0.35	1.429	3.66
$B_{12}C_6N_6$		0.51	1.84	−6.35	−4.51	−5.43	16.02	0.92	0.543	5.43
$B_{12}C_6N_6$@5FU	S_1	4.58	1.80	−5.74	−3.94	−4.84	13.01	0.90	0.556	4.84
$B_{12}C_6N_6$@5FU	S_2	11.73	1.79	−5.33	−3.54	−4.44	10.99	0.90	0.559	4.44

highlights a clear difference among the 5-FU drug and the heteroatom-doped $B_{12}N_{12}$-5FU complexes. The complexes exhibited a decrease in E_g and η values, along with an increase in $\boldsymbol{\sigma}$ and $\boldsymbol{\omega}$ values. These findings indicate that adsorption of the drug onto the nanocages promoted charge transfer and enhanced the complexes' reactivity.

3.7. Density of states (DOS)

The density of states (DOS) and partial density of states (PDOS) served as essential tools in validating interactions between 5-FU and hetero-atom-doped (C, B, and N) $B_{12}N_{12}$ nanocages, as illustrated in Fig. 5. This analysis highlights the fluctuation within the energy gap (E_g) after 5-FU adsorption on different hetero-atom-doped nanocages. DOS analysis represents the energy levels within a system as a continuous molecular property, providing insights into the system's energy distribution. The significant variation in E_g values after 5FU adsorption on C, B, and N-doped $B_{12}N_{12}$ nanocages is notable. The energy gap, E_g range represents electron excitation states, signifying the energy needed for outer-shell electrons to transition into charge carriers, essential for evaluating electrical conductivity. The wanein E_g following the interaction of 5-FU with C, B, and N-doped $B_{12}N_{12}$ nanocages indicates a shift in their behavior toward semiconducting, as illustrated by the DOS investigation shown in Fig. 5.

The DOS interpretation confirmed that during the adsorption of the drug onto hetero-atom-doped $B_{12}N_{12}$ nanocages, the drug molecule contributed to the HOMO while the nanocages contributed to the LUMO, participating in the adsorption fashion. The arrangement of the LUMO orbital demonstrated the significant effect of the PDOS of 5-FU on the TDOS of the complexes. Assessing the LUMO values among several C, B and N doped $B_{12}N_{12}$ nanocages revealed a strong contribution from the C, B, and N-doped $B_{12}N_{12}$ complexes to the adsorption mechanism, suggesting their potential as effective electrochemical sensors. In this study, all nanocages demonstrated bonding features within the DOS range of 4.0 to −16 eV. Furthermore, the Fermi energy levels were estimated as −4.81, −4.80, −4.05, −3.66, and − 4.84 eV for C, B and N doped $B_{12}N_{12}$ nanocage complexes C_{24}@5FU, $B_{12}N_{12}$@5FU, $C_{12}B_6N_6$@5FU, $B_6C_6N_{12}$@5FU and $B_{12}C_6N_6$@5FU complexes, accordingly. The critical insights gained from the DOS analysis are essential for understanding the chemical behavior and adsorption characteristics of C, B, and N-doped $B_{12}N_{12}$ nanocages in relation to their interaction with the 5-FU drug.

3.8. Non-covalent interaction (NCI)

Non-Covalent Interaction (NCI) analysis is essential for investigating the intra- and intermolecular interactions between the drug and nanocages through electron density and its derivatives, which plays a significant role in drug design. To verify the forms of interactions between the 5-FU drug and heteroatom-doped (C, B, and N) $B_{12}N_{12}$ nanocages, we utilized NCI analysis. RDG plots were generated by plotting *S(r)*vs. electron density *ρ(r)*, following the method outlined in Eq. 13 [110].

$$S(r) = \frac{1}{2(3\pi^2)^{1/3}} \frac{|\nabla\rho(r)|}{\rho(r)^{4/3}} \tag{13}$$

The RDG plots, along with the product of the second eigenvalue of the Hessian matrix (λ_2) and electron density ρ (*sign*(λ_2)ρ), were used within the NCI method to examine weak interactions. The adsorption of the 5-FU drug onto heteroatom-doped $B_{12}N_{12}$ nanocages was visualized using 2D scatter plots and 3D color-filled RDG isosurfaces, as presented in Figs.6 and 7. The isosurfaces were color-coded using a blue-green-red scale, corresponding to the values of *sign*(λ_2)ρ. The RDG isosurface was set to a value of 0.60, with *sign*(λ_2)ρ values varying from −0.035 to +0.02 a.u. The interactions are reflected as spikes within this range on the 2D-RDG plots. *Sign*(λ_2)ρ < 0 denotes attractive hydrogen bonding interactions, *sign*(λ_2)ρ > 0 indicates strongly repulsive or steric interactions, and sign(λ_2)ρ ≈ 0 represents weak van der Waals interactions. The color variations on the 3D isosurface plots offer extensive insights into the interaction types, with corresponding colors also appearing on the 2D RDG plots displayed below. Fig. 7 illustrates the 3D color-filled RDG isosurfaces for all the structures analyzed in this study. In every case, disk-shaped green-red isosurfaces develop between the 5-FU molecule and the nanocages, improving the upright alignment of the 5-FU drug while its interaction with the nanocage.

In Fig. 7, the S2 geometry of 5-FU adsorbed on $B_6C_6N_{12}$ and C_{24} nanostructures shows blue spikes in the λ_2 range of approximately −0.02 to −0.03 a.u., indicating strong attractive forces. Alternatively, red spikes appear in the λ_2 range of 0.01 to 0.04 a.u., representing steric repulsions. Green spikes appear in the λ_2 range from 0 to −0.01 a.u., suggesting weak interactions. A few green spikes in the negative λ_2 region likely correspond to weak attractive forces, including van der Waals and dispersion interactions.

In the isosurfaces, green patches signify weak attractive interactions, while blue patches represent strong bonding interactions. Repulsive forces are not visible in the intermolecular isosurfaces but are present in intramolecular surfaces, with red patches only found among identical atoms within the same molecule. This analysis shows that all studied nanostructures exhibit significant non-covalent intra- and intermolecular interactions, with RDG analysis supporting the findings from the NBO study.

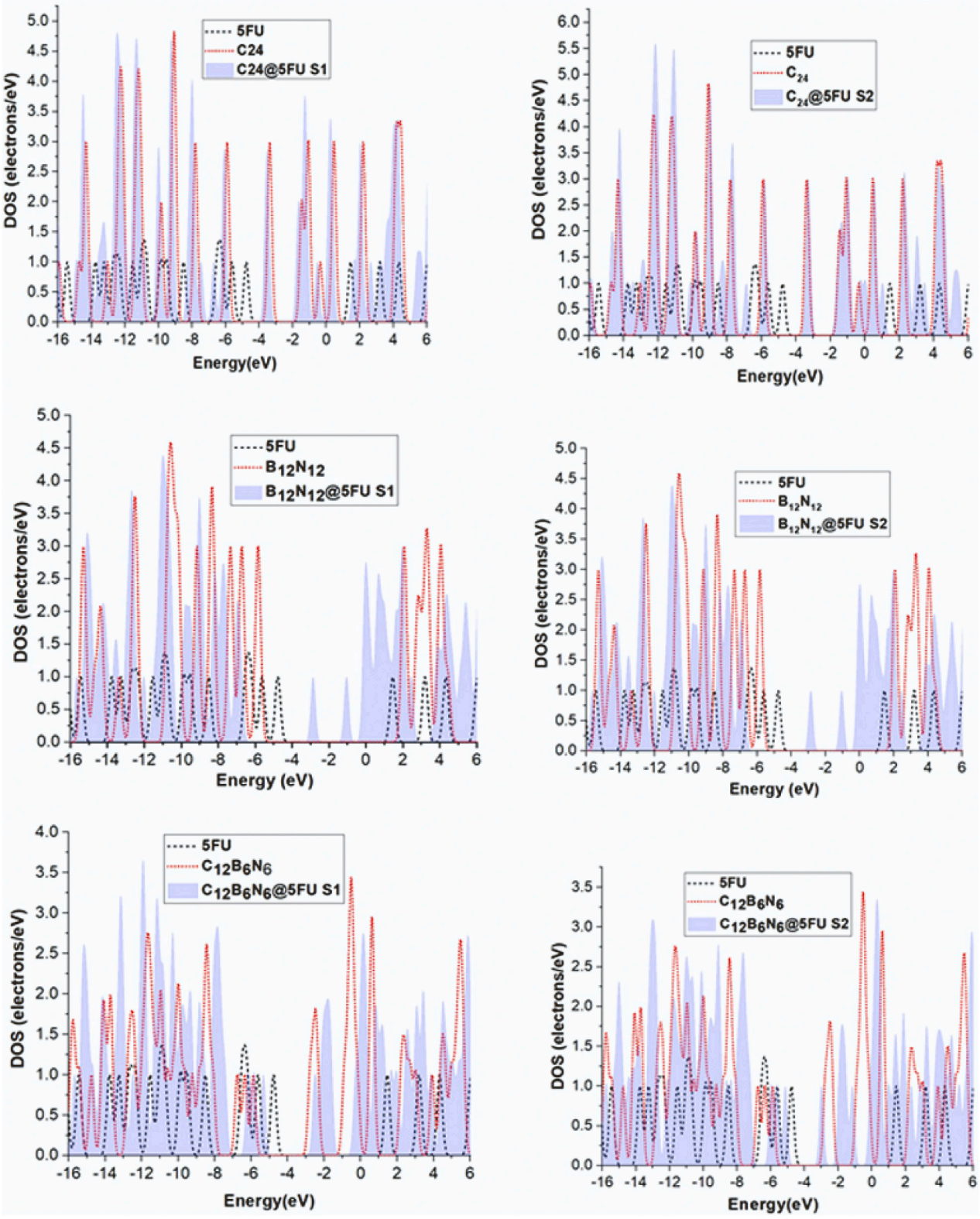

Fig. 5. Partial Density of state (PDOS) of investigated nanocage complexes before and after adsorption.

3.9. Impacts of solvent, drug release mechanism, and molecular dynamics perspectives

All systems, including the drug, nanocages, and their conjugates, were optimized using CPCM. This study assessed how water, a polar medium ($\varepsilon = 78.4$), affects interactions between the drug and nanocage surfaces. Using the formula below, we calculated solvation energy, with negative values indicating the stability and solubility of the studied systems [105].

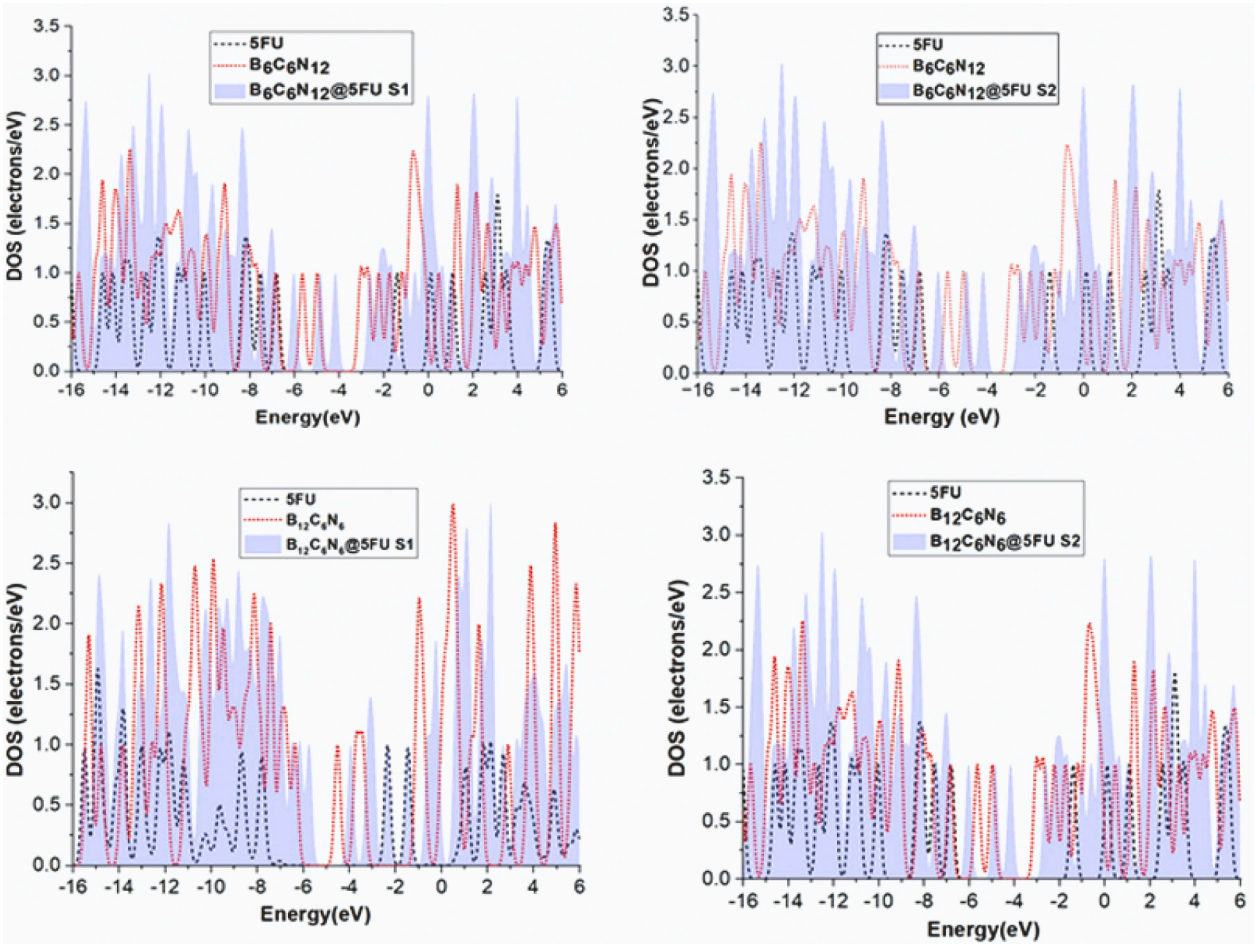

Fig. 5. (*continued*).

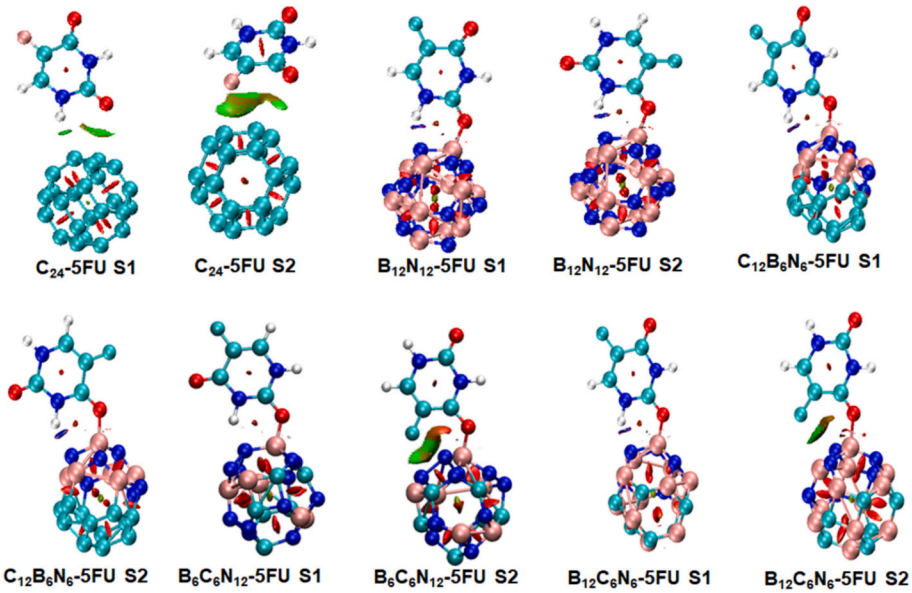

Fig. 6. 2D-RDG scatter plots.

$$E_{sol} = E_{water} - E_{gas} \quad (14)$$

In this context, E_{sol} denotes the system's solvation energy, while E_{water} and E_{gas} represent total energies in water and gas phases, respectively. The adsorption energy (E_{ads}), solvation energy (E_{sol}), dipole moments, and HOMO-LUMO energies of the systems were calculated in solvent phase and presented in Table 5. The calculated solvation energies for the drug and the suggested nanocages were

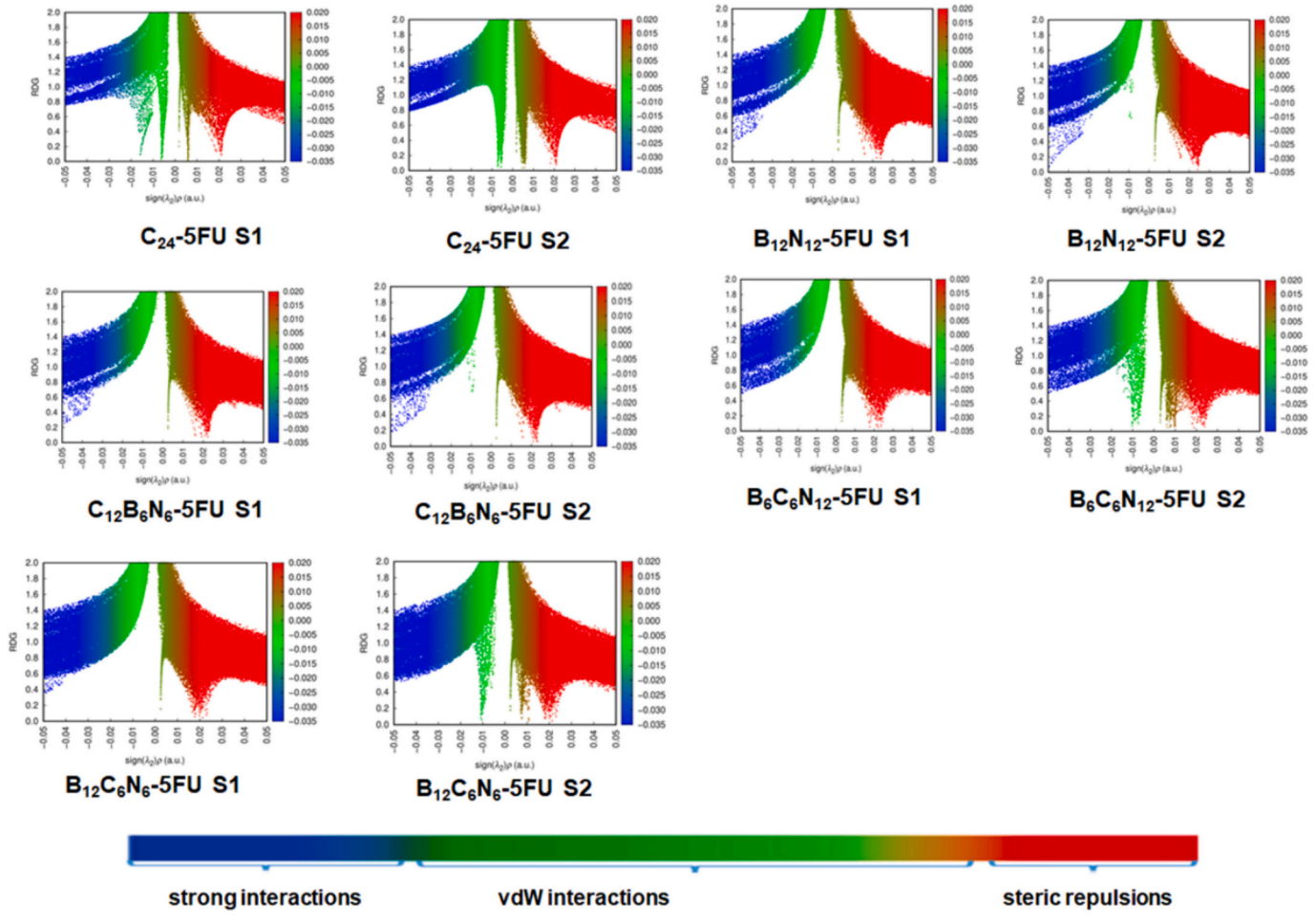

Fig. 7. The 3D color-filled isosurface graphs generated from the grid points for the studied complexes.

Table 5
The adsorption energy; E_{Ads} in kcal mol^{-1}, solvation energy; E_{Sol}, in kcal mol^{-1}, dipole moment in Debye, HOMO energy, E_H in eV; LUMO energy, E_L in eV; energy gap, E_g in eV; change in energy gap, % ΔE_g and recovery time (τ) in second for the investigated complexes in water phase.

Structure	State	E_{ads}	E_{Sol}	D.M.	E_H	E_L	E_g	%ΔE_g	τ (s)
5-FU			−9.70	5.23	−6.61	−1.23	5.38		
C_{24}			−0.65	0.0	−5.83	−3.29	2.54		
C_{24}@5FU	S1	−4.43	−8.93	5.61	−5.83	−3.36	2.47	2.76	1.26×10^{-18} s
C_{24}@5FU	S2	−6.32	−10.12	5.22	−5.77	−3.25	2.52	0.79	2.66×10^{-18} s
$B_{12}N_{12}$			−4.18	0.0	−7.71	−0.79	6.92		
$B_{12}N_{12}$@5FU	S_1	−29.45	−14.50	7.49	−7.06	−1.78	5.28	23.70	4.16×10^{2} s
$B_{12}N_{12}$@5FU	S_2	−29.77	−16.76	15.04	−7.04	−2.28	4.76	31.21	6.97×10^{2} s
$C_{12}B_6N_6$			−3.26	3.06	−5.85	−2.67	3.18		
$C_{12}B_6N_6$@5FU	S_1	−31.43	−13.83	8.89	−5.48	−2.20	3.28	3.14	1.01×10^{4} s
$C_{12}B_6N_6$@5FU	S_2	−31.79	−16.13	17.09	−5.46	−2.34	3.12	1.89	1.81×10^{4} s
$B_6C_6N_{12}$			−7.99	4.23	−5.06	−2.87	2.19		
$B_6C_6N_{12}$@5FU	S_1	−34.11	−12.85	13.43	−4.63	−2.29	2.34	6.85	7.61×10^{5} s
$B_6C_6N_{12}$@5FU	S_2	−34.88	−18.31	16.52	−4.62	−2.50	2.12	3.20	2.63×10^{6} s
$B_{12}C_6N_6$			−2.36	0.76	−6.34	−4.49	1.85		
$B_{12}C_6N_6$@5FU	S_1	−28.37	−12.17	7.86	−5.89	−4.07	1.82	1.62	7.29×10^{1} s
$B_{12}C_6N_6$@5FU	S_2	−22.61	−19.49	17.25	−5.77	−3.96	1.81	2.16	6.76×10^{-3} s

negative, indicating their dissolution in water is energetically favorable and spontaneous [97,105]. Higher solvation energy indicates greater solubility, with the 5-FU-adsorbed $B_6C_6N_{12}$ nanostructures showing the highest values. The adsorption energy of the 5-FU drug with the adsorbents shows only minor differences in the solvent phase relative to the gaseous phase, as shown in Table 5.

The $B_6C_6N_{12}$@5FU bonded S1 geometry parades a slight decrease in adsorption energy in the aqueousphase compared to the gaseous phase, yet it still retains the highest adsorption energy in this study. The $B_6C_6N_{12}$@5FU conjugated geometry with S1 and S2 orientations exhibits strong adsorption in the solvent phase. The hetero-nanocage clusters $B_{12}C_6N_6$ and $C_{12}B_6N_6$ also show promising 5-FU adsorption in certain orientations, but with weaker binding in others.

Additionally, the complexes' dipole moments increase in the solvent phase compared to the gaseous phase, confirming their solubility in polar media. In gas phase, the $B_6C_6N_{12}$@5FU complex showed the highest dipole moment at 13.04 D, followed by $B_{12}C_6N_6$@5FU at 11.73 D, $C_{12}B_6N_6$@5FU at 11.73 D, $B_{12}N_{12}$@5FU at 10.81 D, and C_{24}@5FU at

4.10 D. In water, the dipole moments rose to 17.25 D for $B_{12}C_6N_6$@5FU, 17.09 D for $C_{12}B_6N_6$@5FU, 16.52 D for $B_6C_6N_{12}$@5FU, 15.04 D for $B_{12}N_{12}$@5FU, and 5.61 D for C_{24}@5FU. The increased dipole moments in water confirm that these complexes can dissolve in polar media, boosting their reactivity, which is beneficial for 5-FU drug delivery. Minor differences in HOMO-LUMO energy gaps between the aqueous and gaseous phases also illustrate how solvent media influence the electronic properties of the systems.

The release of drug molecules from carriers plays a vital role in drug delivery, highlighting the significance of assessing recovery time (τ) to evaluate the desorption of 5-FU from $B_{12}N_{12}$ nanocages. This contributes to grasping the effectiveness of nanocages for 5-FU adsorption, as higher E_{ads} values are associated with longer recovery times. For sensor applications, desorption of 5-FU from nanocages can be a limiting factor. According to the research conducted by S. Thomas and M. A. Zaeem [111,112]a shorter recovery time for an adsorbent is advantageous in the design of efficient sensing devices. To assess this, we calculated the recovery time (τ) for drug desorption from the surfaces of $B_{12}N_{12}$ and C-doped $B_{12}N_{12}$ nanocages, following the definition in Eq. 15 [113].

$$\tau = \nu_0^{-1} e^{-E_{ads}} / k_B T \quad (15)$$

The attempt frequency (ν_o), Boltzmann's constant (K_b, approximately 2.0×10^{-3} kcalmol^{-1} K^{-1}), adsorption energy (E_{ads}), and temperature (T) in Kelvin were used to calculate the recovery time (τ) for the desorption of 5-FU drug from C-doped $B_{12}N_{12}$-5FU complexes. In practice, exposure to ultraviolet (UV) light can facilitate the desorption of an adsorbate from the adsorbent. Recovery times were calculated at a temperature of 298.15 K with an attempt frequency (ν) of 10^{18} s^{-1} under UV conditions, as shown in Table 5. Since desorption is the reverse of adsorption, the adsorption energy (E_{ads}) is often considered as the activation energy (E_{activ}) for desorption. However, for a sensor targeting the 5-FU drug, this assumption may not be appropriate, as it leads to an exceptionally long recovery time of 2.63×10^6 s.

The interaction between 5-FU and $B_{12}N_{12}$ and its hetero-atom-doped (C, B, and N) $B_{12}N_{12}$ nanocages $C_{12}B_6N_6$, $B_6C_6N_{12}$ and $B_{12}C_6N_6$ reveals strong physisorption with E_{ads} values between −22.61 and − 34.88 kcal mol^{-1} at solvent phase. The recovery time at 298.15 K(room temperature) for 5-FU adsorbed onto these nanocages ranges from 6.76×10^{-3} s to 2.62×10^6 s except C_{24} surface which has 2.6×10^{-18} s, indicating a moderate interaction, preventing 5-FU's spontaneous desorption from these nanocages, making it a potential drug carrier.

We have performed constant –pH MD and protonation –dependent DFT to better understand pH-triggered drug release and kinetics under acidic conditions. We investigated the pH-responsive behavior by simulating protonation at the O_7 site of 5-FU in the $B_6C_6N_{12}$-5FU (S1) and $B_{12}C_6N_6$-5FU (S1) systems. These simulations were designed to replicate the acidic tumor microenvironment (pH < 6) and compare it with physiological conditions (pH 7.35–7.45). As illustrated in Fig.8, the B—O_7 bond length expanded markedly-from 1.51 Å and 1.55 Å to 11.35 Å and 10.80 Å, respectively-indicating a substantial weakening of the drug–nanocage interaction under acidic conditions. Correspondingly, the adsorption energy (E_{ads}) decreased from −38.94 kcal mol^{-1} and -30.55 kcal mol^{-1}, providing strong evidence of pH-triggered release of 5-FU from the $B_6C_6N_{12}$ and $B_{12}C_6N_6$ nanocarriers in tumor-like environments.

Drug adsorption and release were also simulated under biological conditions by placing $B_{12}N_{12}$-5FU, $C_{12}B_6N_6$-5FU, $B_6C_6N_{12}$-5FU and $B_{12}C_6N_6$-5FU complexes in water and acidic environments. The solvation energy was calculated using the CPCM, expressed as the difference between the total energies in the aqueous and gas phases. Under acidic conditions, the oxygen atom of 5-FU is protonated in both complexes (Fig. S2), enabling pH-triggered drug release between normal and target cells. DFT calculations were conducted to investigate mechanism of drug release from the $B_{12}N_{12}$, $C_{12}B_6N_6$, $B_6C_6N_{12}$, and $B_{12}C_6N_6$ nanocage complexes, highlighting their potential in drug delivery applications. To further investigate solvent effects, four water molecules were positioned at the interaction sites of these complexes, and the interaction energies of water and nanocages were calculated utilizing $E_{abs}(H_2O–BN) = (E_{H_2O/BN} - (E_{H_2O} + E_{BN}) + E_{BSSE})/4$. Table S3 presents solvent energies, water-hetero-fullerene interaction energies, and adsorption energies for $B_{12}N_{12}$-5FU, $C_{12}B_6N_6$-5FU and $B_{12}C_6N_6$-5FU complexes. The interactions between water and the nanocages were found to be much weaker than the interactions between 5-FU and the nanocages, indicating that the adsorption of 5-FU is only slightly impressed by the presence of water molecules. The negative adsorption energies in both gas and aqueous phases confirm the beneficial and spontaneous interactions between 5-FU and heteroatom-doped $B_{12}N_{12}$ nanocages.

The $B_6C_6N_{12}$-5FU bonded S1 geometry exhibits a slight decrease in adsorption energy in the aqueous phase in comparison to the gas phase, however it still holds the highest adsorption energy observed in this

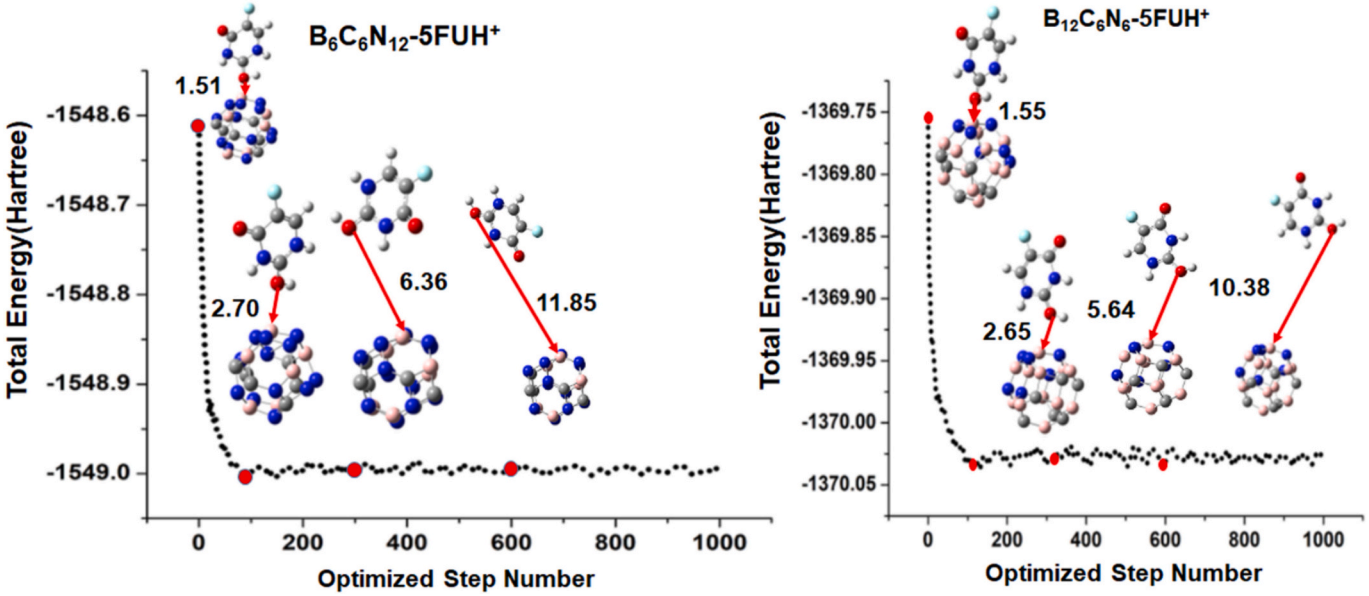

Fig. 8. Optimization process and corresponding bond lengths (in Å) of protonated APN adsorbed on decorated $B_6C_6N_{12}$-5FU and $B_{12}C_6N_6$-5FU in acidic conditions, where the red dots correspond to relevant structure.

study. Both S1 and S2 orientations of the $B_6C_6N_{12}$-5FU conjugated structure demonstrate strong adsorption behavior in the water phase. Additionally, hetero-nanocage clusters like $B_{12}C_6N_6$ and $C_{12}B_6N_6$ also show promising adsorption potential for 5-FU, although the binding strength varies by orientation and is generally weaker in certain configurations.

To assess stability and interactions between the drug and nanocages, ADMP dynamics were applied to the most effective drug-adsorbent nanocages at room temperature (300*K*) in an aqueous environment. The ADMP simulations, run over a 1000 fs using a 2 fs time step per frame, reveal minor fluctuations in total energy without any bond dissociation or separation of fragments throughout the simulation (as illustrated in Figs. 9 and S3). We agree that the total simulated time of 1000 fs (1 ps) represents a relatively short timescale and, by itself, may not be sufficient to fully confirm long-term stability or chemical affinity. We have also performed an additional 5000 fs (5 ps**)** ADMP simulation to further examine whether the drug desorbs from the nanocage surface. The results, demonstrating that the complex remains stable and no desorption occurs throughout the extended simulation, are presented in Fig. S4. These findings suggest the high chemical affinity and stability, indicating the nanocages could serve as effective carriers for the 5-FU drug in biological or aqueous environments.

3.10. Infrared (IR) and raman spectra

To further elucidate the 5-FU loading mechanism, the IR and Raman spectra of the pristine and hybrid nanocages and their 5-FU complexes were analyzed and presented in Figs. S5 and S6. The IR spectra revealed noticeable shifts in the stretching vibration bands upon 5-FU adsorption, indicating strong interactions between the drug and the nanocages. Additionally, the emergence of new absorption bands confirmed the formation of stable adsorption complexes. The Raman spectra also exhibited distinct variations after 5-FU adsorption, demonstrating the influence of the drug on the vibrational characteristics of the nanocages [114–116]. Notably, several modes that were inactive in the free 5-FU spectrum became active in the 5-FU–nanocage complexes, further validating the interaction. These spectral observations collectively suggest that the studied nanocages possess significant potential as effective drug delivery carriers for 5-FU.

3.11. UV spectra simulation using TD-DFT calculations

Time-dependent density functional theory (TD-DFT) calculations were used to generate the ultraviolet-visible (UV–Vis) spectra for all nanocage complexes studied, assessing the effect of 5-FU binding to the proposed adsorbents. These calculations were performed using TD-DFT at the B3LYP-GD3(BJ)/6–31 + G(d,p) level of theory, considering up to 30 excited states both gas and water phase. Figs. 10 and S7 display the simulated UV–vis spectra both before and after adsorption. Additionally, the maximum oscillator strength, corresponding wavelengths, energy, and transitions calculated by TD-DFT are listed in Table S5 and S6. UV–vis spectroscopy is widely used for tracking drug concentration and monitoring interactions.

The simulated spectra analysis shows a significant shift in the maximum absorption coefficient after 5-FU adsorption on the adsorbent surfaces. In most cases, there is a red shift in the wavelength associated with the highest absorbance after adsorption. For instance, in the $B_{12}N_{12}$@5FU conjugated structures, the initial maximum absorption peaks for the 5-FU drug and $B_{12}N_{12}$ nanocage were around 162 nm and 194 nm, respectively. After adsorption, the peaks shifted to 249 nm and 274 nm for the S1 and S2 geometries, respectively, indicating significant changes in the electronic and chemical states of both the drug and nanocages, thus confirming the adsorption mechanism.

Additionally, the variations in oscillator strength following

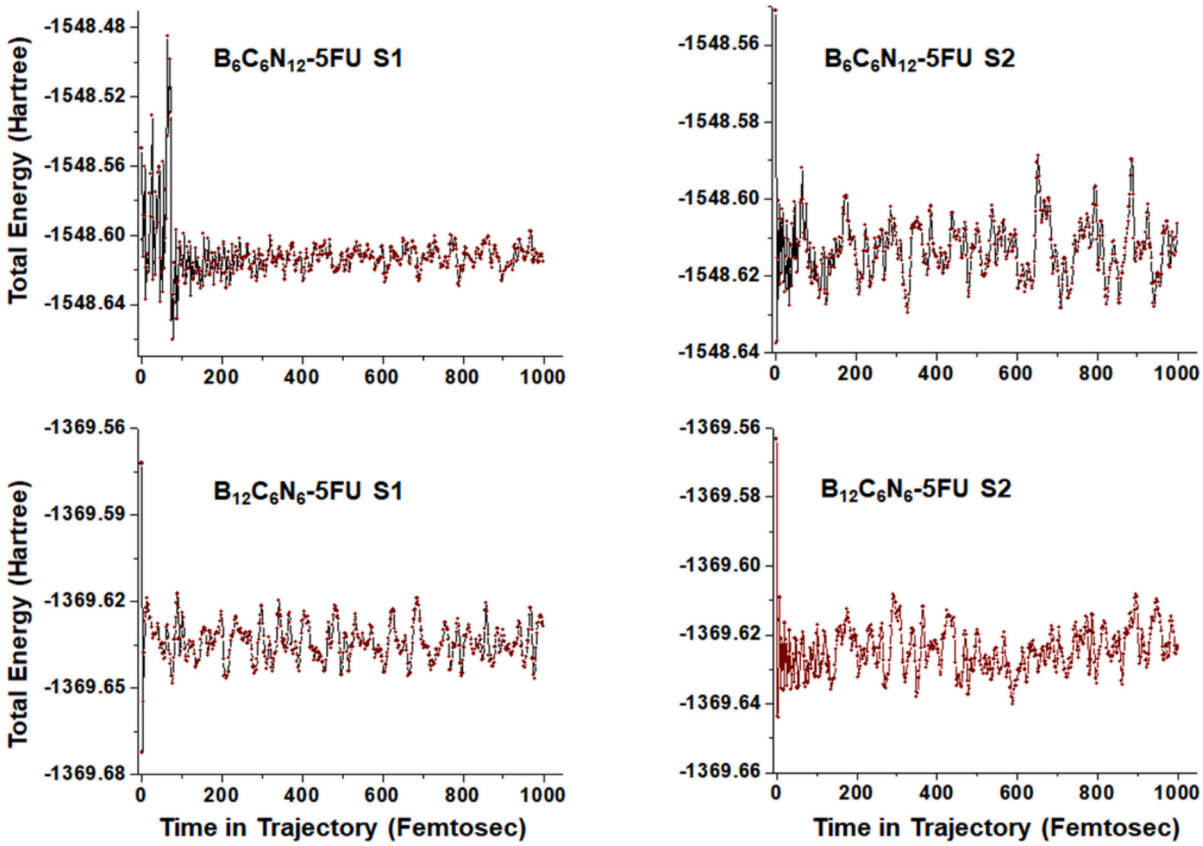

Fig. 9. ADMP molecular dynamics trajectories for 1000 fs for $B_6C_6N_{12}$@5FU (S1 & S2) and $B_{12}C_6N_6$@5FU (S1 & S2) complexes.

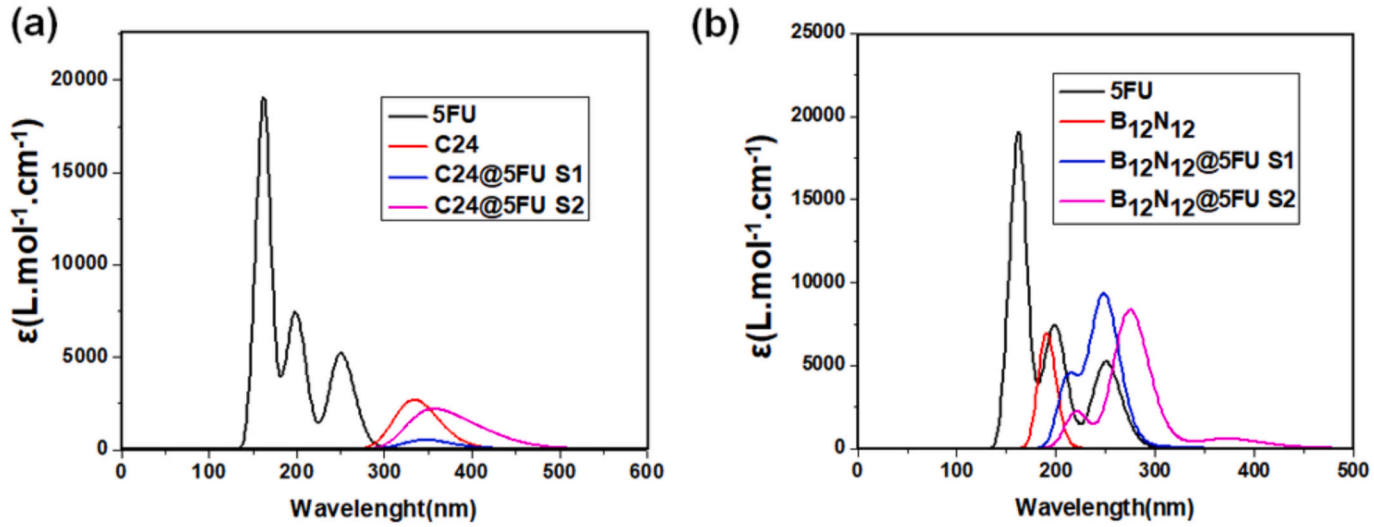

Fig. 10. Simulated UV–Vis spectra of systems before and after adsorption of C_{24}@5FU and $B_{12}N_{12}$@5FU complexes.

adsorption are clearly presented in Table S6, with the $C_{12}B_6N_6$@5FU S2 structure exhibiting the highest oscillator strength of 0.1378, resulting from an electron transition from the ground state (S_0) to the 26th state (S_{26}). These findings suggest that UV–Vis spectroscopy could serve as an effective tool for monitoring the interaction between the 5-FU drug and the nanocages, allowing researchers to track changes in concentration and binding events. This transformation in the spectra not only validates the occurrence of adsorption but also reveals deeper insights into the nature of the interactions taking place at a molecular level.

4. Conclusions

This study investigates the sensitivity, reactivity, and adsorption potential of pristine C_{24}, $B_{12}N_{12}$, and hybrid nanocages ($C_{12}B_6N_6$, $B_6C_6N_{12}$, and $B_{12}C_6N_6$) toward 5-fluorouracil (5-FU) in gas and aqueous phases. Adsorption energies (E_{ads}) and BSSE-corrected deformation energies reveal stronger binding in hybrid nanocages, with $B_6C_6N_{12}$ exhibiting the highest adsorption energy of −38.94 kcal mol^{-1} compared to pristine nanocages (−6.54 and − 28.82 kcal mol^{-1} for C_{24} and $B_{12}N_{12}$). Thermodynamic analysis shows spontaneous, exothermic adsorption for all except C_{24}@5-FU, with $B_6C_6N_{12}$@5-FU having the most favorable Gibbs free energy change ($\Delta G = -34.87$ kcal mol^{-1}) at 298 K. Frontier molecular orbital (FMO) and density of states (DOS) analyses show energy gap reductions of 43 % for $B_{12}N_{12}$ and 64 % for $B_6C_6N_{12}$ post-adsorption, indicating enhanced electronic sensitivity. Natural bond orbital (NBO) analysis confirms significant charge transfer (~ − 0.31e) from 5-FU to nanocages. Non-covalent interaction (NCI) and reduced density gradient (RDG) analyses highlight dominant van der Waals and electrostatic forces, with no repulsive interactions detected. UV–Vis spectral simulations reveal notable shifts in absorbance and oscillator strength upon 5-FU binding. Polarized continuum model (PCM) and ADMP molecular dynamics validate improved solubility and complex stability in aqueous media. Overall, $B_6C_6N_{12}$ shows the strongest, most stable binding with 5-FU, indicating high potential as a nanocarrier for drug delivery, reducing side effects, and offering promising applications in nanomedicine. These quantitative findings pave the way for experimental validation and development of heterofullerene-based 5-FU delivery systems.

CRediT authorship contribution statement

Mohammad A. Matin: Writing – review & editing, Writing – original draft, Visualization, Supervision, Project administration, Investigation, Formal analysis, Data curation, Conceptualization. **Md. Alauddin:** Writing – original draft, Visualization. **Tapas Debnath:** Writing – original draft, Visualization, Formal analysis. **Abu Asaduzzaman:** Visualization, Formal analysis. **Joonkyung Jang:** Visualization, Conceptualization.

Declaration of competing interest

The authors declare that they have no known competing financial interests or personal relationships that could have appeared to influence the work reported in this paper.

Acknowledgements

The authors sincerely thanks the Computing Research Laboratory, CARS, DU, for the support in this research.

Appendix A. Supplementary data

Supplementary data to this article can be found online at https://doi.org/10.1016/j.diamond.2025.113095.

Data availability

The data that has been used is confidential.

References

[1] P. Kesharwani, R. Ghanghoria, N.K. Jain, Carbon nanotube exploration in cancer cell lines, Drug Discov. Today 17 (2012) 1023–1030.
[2] C.Y. Ang, S.Y. Tan, Y. Zhao, Recent advances in biocompatible nanocarriers for delivery of chemotherapeutic cargoes towards cancer therapy, Org. Biomol. Chem. 12 (2014) 4776–4806.
[3] E. Duverger, T. Gharbi, E. Delabrousse, F. Picaud, Quantum study of boron nitride nanotubes functionalized with anticancer molecules, Phys. Chem. Chem. Phys. 16 (2014) 18425–18432.
[4] J. Li, R. Wang, J. Gao, Novel anticancer drugs approved in 2020, Drug discoveries & therapeutics 15 (2021) 44–47.
[5] N.M. Kuderer, T.K. Choueiri, D.P. Shah, Y. Shyr, S.M. Rubinstein, D.R. Rivera, S. Shete, C.Y. Hsu, A. Desai, G. de Lima Lopes Jr., P. Grivas, C.A. Painter, S. Peters, M.A. Thompson, Z. Bakouny, G. Batist, T. Bekaii-Saab, M.A. Bilen, N. Bouganim, M.B. Larroya, D. Castellano, S.A. Del Prete, D.B. Doroshow, P. C. Egan, A. Elkrief, D. Farmakiotis, D. Flora, M.D. Galsky, M.J. Glover, E. A. Griffiths, A.P. Gulati, S. Gupta, N. Hafez, T.R. Halfdanarson, J.E. Hawley, E. Hsu, A. Kasi, A.R. Khaki, C.A. Lemmon, C. Lewis, B. Logan, T. Masters, R. R. McKay, R.A. Mesa, A.K. Morgans, M.F. Mulcahy, O.A. Panagiotou, P. Peddi, N. A. Pennell, K. Reynolds, L.R. Rosen, R. Rosovsky, M. Salazar, A. Schmidt, S. A. Shah, J.A. Shaya, J. Steinharter, K.E. Stockerl-Goldstein, S. Subbiah, D.C. Vinh, F.H. Wehbe, L.B. Weissmann, J.T. Wu, E. Wulff-Burchfield, Z. Xie, A. Yeh, P.P. Yu, A.Y. Zhou, L. Zubiri, S. Mishra, G.H. Lyman, B.I. Rini, J.L. Warner, Clinical impact

of COVID-19 on patients with cancer (CCC19): a cohort study, Lancet (London, England) 395 (2020) 1907–1918.
[6] S. Jia, R. Wang, K. Wu, H. Jiang, Z. Du, Elucidation of the mechanism of action for metal based anticancer drugs by mass spectrometry-based quantitative proteomics, Molecules (Basel, Switzerland) 24 (2019).
[7] G. Yu, D.N. Wu, Y. Yu, G.F. Li, H.H. Zhou, Impact of dosage timing on the bioavailability of oral anticancer medications: Is pre-prandial dosing equivalent to post-prandial dosing, Journal of oncology pharmacy practice: official publication of the International Society of Oncology Pharmacy Practitioners 25 (2019) 404–408.
[8] A. Khajeh, H. Modarress, Effect of cholesterol on behavior of 5-fluorouracil (5-FU) in a DMPC lipid bilayer, a molecular dynamics study, Biophys. Chem. 187-188 (2014) 43–50.
[9] C.-H. Wu, C.-C. Wu, Y.-S. Ho, Antitumor activity of combination treatment of *Lentinus edodes* mycelium extracts with 5-fluorouracil against human colon cancer cells xenografted in nude mice, J. Cancer Mol. 3 (2007) 15–22.
[10] K. Zare, F. Najafi, H. Sadegh, R.S. Ghoshekandi, Studies of ab initio and Monte Carlo simulation on interaction of fluorouracil anticancer drug with carbon nanotube, J. Nanostructure Chem. 3 (2013) 1–8.
[11] P.M. Wigmore, S. Mustafa, M. El-Beltagy, L. Lyons, J. Umka, G. Bennett, Effects of 5-FU, Adv. Exp. Med. Biol. 678 (2010) 157–164.
[12] D. Peer, J.M. Karp, S. Hong, O.C. Farokhzad, R. Margalit, R. Langer, Nanocarriers as an emerging platform for cancer therapy, Nat. Nanotechnol. 2 (2007) 751–760.
[13] T.C. Johnstone, K. Suntharalingam, S.J. Lippard, The next generation of platinum drugs: targeted Pt (II) agents, nanoparticle delivery, and Pt (IV) prodrugs, Chem. Rev. 116 (2016) 3436–3486.
[14] R. Singh, J.W. Lillard Jr., Nanoparticle-based targeted drug delivery, Exp. Mol. Pathol. 86 (2009) 215–223.
[15] S.H. Friedman, D.L. DeCamp, R.P. Sijbesma, G. Srdanov, F. Wudl, G.L. Kenyon, Inhibition of the HIV-1 protease by fullerene derivatives: model building studies and experimental verification, J. Am. Chem. Soc. 115 (1993) 6506–6509.
[16] L.L. Dugan, D.M. Turetsky, C. Du, D. Lobner, M. Wheeler, C.R. Almli, C.K. Shen, T.Y. Luh, D.W. Choi, T.S. Lin, Carboxyfullerenes as neuroprotective agents, Proc. Natl. Acad. Sci. USA 94 (1997) 9434–9439.
[17] D.W. Cagle, S.J. Kennel, S. Mirzadeh, J.M. Alford, L.J. Wilson, In vivo studies of fullerene-based materials using endohedral metallofullerene radiotracers, Proc. Natl. Acad. Sci. USA 96 (1999) 5182–5187.
[18] A. Montellano, T. Da Ros, A. Bianco, M. Prato, Fullerene C60 as a multifunctional system for drug and gene delivery, Nanoscale 3 (2011) 4035–4041.
[19] S.A. Andujar, F. Lugli, S. Höfinger, R.D. Enriz, F. Zerbetto, Amyloid-β fibril disruption by C60—molecular guidance for rational drug design, Phys. Chem. Chem. Phys. 14 (2012) 8599–8607.
[20] L. Ahmed, B. Rasulev, M. Turabekova, D. Leszczynska, J. Leszczynski, Receptor- and ligand-based study of fullerene analogues: comprehensive computational approach including quantum-chemical, QSAR and molecular docking simulations, Org. Biomol. Chem. 11 (2013) 5798–5808.
[21] Y. Lai, T.J. Al-Musawi, U. Abdul-Reda Hussein, I. Waleed, H. Hassan Ahmed, A. Qasim Khallawi, K. Majid Alsaraf, M. Asiri, M. Abosaooda, H.O. Alsaab, A first-principal study of pure and encapsulation boron nitride cluster with alkaline metals as the metformin drug carrier, J. Mol. Liq. 384 (2023) 122260.
[22] M.A.A. Ibrahim, A.-s.S.M. Rady, N.A.M. Moussa, M.N. Ahmed, P.A. Sidhom, A. M. Shawky, A.M. Alqahtani, L.A. Mohamed, Investigation of aluminum nitride nanocarrier for drug delivery process of Favipiravir: a DFT study, J. Mol. Liq. 372 (2023) 121209.
[23] M. Pishnamazi, S.M. Alshahrani, H. Faris Alotaibi, The roles of gold and platinum decoration and trapping on the B12N12 fullerene in improving the antitumor efficacy of ifosfamide: A DFT and spectroscopic study, J. Mol. Liq. 410 (2024) 125541.
[24] M.R. Sameti, M. Torkashvand, Theoretical evaluation of C24 nanocage functionalization with protons for enhanced sulfacetamide drug delivery: A DFT study with non-covalent interaction analyses, J. Mol. Struct. 1318 (2024) 139298.
[25] A.U. Rahman, D.M. Saaduzzaman, S.M. Hasan, M.K.U. Sikder, Feasibility of nitride-based nanocages for the targeted delivery of ifosfamide: a DFT exploration, New J. Chem. 48 (2024) 15599–15609.
[26] M.Y. Mehboob, R. Hussain, F. Younas, S. Jamil, M.M.A. Iqbal, K. Ayub, N. Sultana, M.R.S.A. Janjua, Computation Assisted Design and Prediction of Alkali-Metal-Centered B12N12 Nanoclusters for Efficient H2 Adsorption: New Hydrogen Storage Materials, J. Clust. Sci. 34 (2023) 1237–1247.
[27] C. Lee, Y. Seo, J. Han, J. Hwang, I. Jeon, Perspectives on critical properties of fullerene derivatives for rechargeable battery applications, Carbon 210 (2023) 118041.
[28] K. Guo, N. Li, L. Bao, X. Lu, Fullerenes and derivatives as electrocatalysts: Promises and challenges, Green Energy & Environment 9 (2024) 7–27.
[29] A.A. Oishi, P. Dhali, A. Das, S. Mondal, A.S. Rad, M.M. Hasan, Study of the adsorption of chloropicrin on pure and Ga and Al doped B12N12: a comprehensive DFT and QTAIM investigation, Mol. Simul. 48 (2022) 776–788.
[30] A. Kausar, I. Ahmad, M. Maaza, M.H. Eisa, P. Bocchetta, Polymer/Fullerene Nanocomposite for Optoelectronics—Moving toward Green Technology, J. Compos. Sci. 6 (2022) 393.
[31] M.G. Muktadir, A. Alam, A.A. Piya, S.U.D. Shamim, Exploring the adsorption ability with sensitivity and reactivity of C12–B6N6, C12–Al6N6, and B6N6–Al6N6 heteronanocages towards the cisplatin drug: a DFT, AIM, and COSMO analysis, RSC Adv. 12 (2022) 29569–29584.
[32] X. Li, L. Yang, X. Sun, A comparative study of the carbon-based nanostructures for the delivery and detection of drug metronidazole, Diam. Relat. Mater. 149 (2024) 111562.
[33] T. Oku, A. Nishiwaki, I. Narita, Formation and atomic structure of B12N12 nanocage clusters studied by mass spectrometry and cluster calculation, Sci. Technol. Adv. Mater. 5 (2004) 635–638.
[34] K. Hachem, M. Jade Catalan Opulencia, W. Kamal Abdelbasset, A. Sevbitov, O. R. Kuzichkin, A. Mohamed, S. Moazen Rad, A. Salehi, J. Kaur, R. Kumar, A. Ng Kay Lup, A. Arian Nia, RETRACTED: Anti-inflammatory effect of functionalized sulfasalazine boron nitride nanocages on cardiovascular disease and breast cancer: an in-silico simulation, J. Mol. Liq. 356 (2022) 119030.
[35] K. Chukwuemeka, H. Louis, I. Benjamin, P.A. Nyong, E.U. Ejiofor, E.A. Eno, A.-L. E. Manicum, Therapeutic Potential of B12N12-X (X = Au, Os, and Pt) Nanostructured as Effective Fluorouracil (5Fu) Drug Delivery Materials, ACS Appl. Bio Mater. 6 (2023) 1146–1160.
[36] A. Soltani, A. Sousaraei, M. Bezi Javan, M. Eskandari, H. Balakheyli, Electronic and optical properties of 5-AVA-functionalized BN nanoclusters: a DFT study, New J. Chem. 40 (2016) 7018–7026.
[37] F. Azarakhshi, S. Shahab, S. Kaviani, M. Sheikhi, Investigation of Adsorption of Sulfanilamide Drug on Surfaces of the B12N12 and Al12N12 Fullerenes: A DFT Study, Lett. Org. Chem. 18 (2021) 640–655.
[38] R. Padash, M.R. Esfahani, A.S. Rad, The computational quantum mechanical study of sulfamide drug adsorption onto X12Y12 fullerene-like nanocages: detailed DFT and QTAIM investigations, J. Biomol. Struct. Dyn. 39 (2021) 5427–5437.
[39] S. Lin, X. Wang, Y. Yang, X. Meng, Y. Qu, Y.-Q. Li, M. Zhao, X. Liu, W. Li, Sub-nanometer-sized carbon nanoparticle shows higher biocompatibility to DNA than nanometer-sized nanoparticles, J. Phys. D. Appl. Phys. 55 (2022) 295401.
[40] A. Merlo, V.R.S.S. Mokkapati, S. Pandit, I. Mijakovic, Boron nitride nanomaterials: biocompatibility and bio-applications, Biomater. Sci. 6 (2018) 2298–2311.
[41] A.K. Vishwkarma, T. Yadav, A. Pathak, G. Brahmachari, Interaction of a synthetic bio-relevant drug-molecule with C24 and B12N12 fullerene: A first-principles quantum chemical investigation, Diam. Relat.Mater. 132 (2023) 109639.
[42] A. Hosseinian, E. Vessally, S. Yahyaei, L. Edjlali, A. Bekhradnia, A Density Functional Theory Study on the Interaction Between 5-Fluorouracil Drug and C24 Fullerene, J. Clust. Sci. 28 (2017) 2681–2692.
[43] R. Guo, Q. Liu, W. Wang, R. Tayebee, F. Mollania, Boron nitride nanostructures as effective adsorbents for melphalan anti-ovarian cancer drug. Preliminary MTT assay and in vitro cellular toxicity, J. Mol. Liq. 325 (2021) 114798.
[44] M. Kurban, İ. Muz, Theoretical investigation of the adsorption behaviors of fluorouracil as an anticancer drug on pristine and B-, Al-, Ga-doped C36 nanotube, J. Mol. Liq. 309 (2020) 113209.
[45] N. Abdolahi, P. Singla, A. Soltani, M. Javan, M. Aghaei, F. Heidari, S. Sedighi, Gold decorated B12N12 nanocluster as an effective sulfasalazine drug carrier: A theoretical investigation, Phys. E: Low-dimensional Syst. Nanostruct. 124 (2020) 114296.
[46] C.Y. Hsu, M.J. Saadh, A.I. Ayesh, M.D. El-Muraikhi, M. Mirzaei, M. Da'i, S. Ghotekar, M.M. Salem-Bekhit, Exploring the naproxen adsorption at the surface of iron-decorated C24 fullerene-like nanocages for providing drug delivery insights along with DFT calculations, Diam. Relat. Mater. 146 (2024) 111262.
[47] A. Soltani, M.R. Taghartapeh, V. Erfani-Moghadam, M.B. Javan, F. Heidari, M. Aghaei, P.J. Mahon, Serine adsorption through different functionalities on the B12N12 and Pt-B12N12 nanocages, Mater. Sci. Eng. C 92 (2018) 216–227.
[48] İ. Muz, Enhanced adsorption of fluoroquinolone antibiotic on the surface of the Mg-, Ca-, Fe- and Zn-doped C60 fullerenes: DFT and TD-DFT approach, Mater Today Commun 31 (2022) 103798.
[49] M.J. Saadh, S.M. Dhiaa, A.H.A. Hussein, M.M. Karim, A.H. Idan, M. Mirzaei, S. A. Mosaddad, M.M. Salem-Bekhit, Exploring smart drug delivery platforms through the adsorption of chlormethine anticancer by an iron-enhanced metallofullerene, J. Indian Chem. Soc. 101 (2024) 101294.
[50] C.-Y. Hsu, A.H. Jabbar, A.H. Shather, A.S. Alkhayyat, A. Alsalamy, A.K. Hamad, N.M. Ahmed, Z.H. Mahmoud, Z.T. Abed, Utility of (MgO)12 nanocage as a chemical sensor for recognition of amphetamine drug: a computational inspection, Chemical Physics Impact 7 (2023) 100382.
[51] X. Yao, J. Mu, Y. Zheng, J. Wu, W. Zhu, K. Wang, Tailoring the adsorption behaviors of flucytosine on BnNn (n = 12, 16, 20, and 24) nanocage scaffolds: A computational insight on drug delivery applications, Colloids Surf. A Physicochem. Eng. Asp. 678 (2023) 132481.
[52] S.U.D. Shamim, M.H. Miah, M.R. Hossain, M.M. Hasan, M.K. Hossain, M. A. Hossain, F. Ahmed, Theoretical investigation of emodin conjugated doped B12N12 nanocage by means of DFT, QTAIM and PCM analysis, Phys. E Low-Dimens. Syst. Nanostruct. 136 (2022) 115027.
[53] P. Dhali, A.K.M.A. Hossain, Investigating the adsorption potential and sensitivity of pristine along with carbon, boron, and nitrogen substituted hetero-nanocages towards azacitidine drug, J. Mol. Liq. 396 (2024) 124051.
[54] G. Mehraein, M. Rezaei-Sameti, E. Asgary, M. Aghamohammadi, The effects of Cu, Zn doped, and static electrical field on the interaction of mercaptopyridine drug with B12P12 nanocage: insight from DFT, TD-DFT, J. Mol. Struct. 1248 (2022) 131478.
[55] Y. Cao, A. Khan, H. Mirzaei, S. Reza Khandoozi, M. Javan, A. Ng Kay Lup, A. Norouzi, E. Tazikeh Lemeski, M. Pishnamazi, A. Soltani, A.B. Albadarin, Investigations of adsorption behavior and anti-cancer activity of curcumin on pure and platinum-functionalized B12N12 nanocages, J. Mol. Liq. 334 (2021) 116516.

[56] M. Suliman, M. Hadi Kzar, A.S.M. Juma, I. Abbas Ali, Y. Yasin, N. Hassan Sayyid, A. Taan Alkhafaji, A.J. Kadhim, M.M. Abid, A. Hussien Alawadi, A. Alsalamy, J. Kaur, E. Tazikeh-Lemeski, S. Moazen Rad, A. Soltani, B40 and SiB39 fullerenes enhance the physicochemical features of curcumin and effectively improve its anti-inflammatory and anti-cancer activities, J. Mol. Liq. 395 (2024) 123816.
[57] M. Khaleghian, M. Sheikhi, S. Shahab, S. Kaviani, Investigation of adsorption behavior of penicillamine anticancer drug upon B12P12, Ga12P12, and B6Ga6P12 fullerene-like nano-cages: a DFT insight, Comput. Theor. Chem. 1237 (2024) 114616.
[58] M.A. Matin, M. Alauddin, M.M. Islam, Investigation of transition metals (Ag, Au, Pd, Pt and Ru)-doped boron nitride nanocarrier for drug delivery process of favipiravir: An intuition from DFT, J. Mol. Liq. 407 (2024) 125244.
[59] M.A. Matin, J.K. Saha, T. Debnath, J. Jang, Exploring the interaction of Cu-modified B12N12 nanocages for Favipiravir drug delivery using density functional theory study, J. Mol. Liq. 414 (2024) 125999.
[60] M.J. Saadh, M. Mirzaei, Z.S. Ghnim, S.A. Mosaddad, M.M. Salem-Bekhit, Density functional theory analyses of an iron-doped nanocage for the adsorption of allopurinol drug towards the development of novel carriers, Comput. Theor. Chem. 1237 (2024) 114664.
[61] Z. Liao, G. Song, Z. Yang, H. Ren, Adsorption and desorption behaviors of hydroxyurea drug on delivery systems of B12N12 fullerene and its Al-, Si- and P-dopings from theoretical perspective, Mol. Phys. 119 (2021) e1921296.
[62] A. Gholami, E. Shakerzadeh, E. Chigo Anota, M. corazon Flores Bautista, A theoretical perspective on the adsorption performance of pristine and Metal-encapsulated B36N36 fullerenes toward the hydroxyurea and nitrosourea anticancer drugs, Inorg. Chem. Commun. 148 (2023) 110326.
[63] A.A. Piya, A.K.M.A. Hossain, Investigation of the adsorption behavior of the anti-cancer drug hydroxyurea on the graphene, BN, AlN, and GaN nanosheets and their doped structures via DFT and COSMO calculations, RSC Adv. 13 (2023) 27309–27320.
[64] Z.M. Shabavi, E. Shakerzadeh, T. Yadav, E. Tahmasebi, S. Kaviani, E.C. Anota, A DFT study on the potential application of metal-encapsulated B12N12 nanocage for efficient removal of gemifloxacin in aqueous medium, Comput. Theor. Chem. 1234 (2024) 114535.
[65] Z.M. Shabavi, E. Shakerzadeh, T. Yadav, E.C. Anota, Quantum chemical insights into the adsorption performance of pristine and M-encapsulated (M = Li, Na, K) B12N12 nanocages toward ciprofloxacin, levofloxacin, moxifloxacin, delafloxacin and ofloxacin antibiotics, Diam. Relat. Mater. 148 (2024) 111463.
[66] H.O. Edet, H. Louis, T.E. Gber, P.S. Idante, T.C. Egemonye, P.B. Ashishie, E. E. Oyo-Ita, I. Benjamin, A.S. Adeyinka, Heteroatoms (B, N, S) doped quantum dots as potential drug delivery system for isoniazid: insight from DFT, NCI, and QTAIM, Heliyon 9 (2023) e12599.
[67] M. Sadat Mussavi, S. Hosseini, DFT study on the potential of M@B40 (M = Mg and K) metalloborospherenes as nanocarrier for 6-Thioguanine anticancer drug, J. Mol. Liq. 395 (2024) 123900.
[68] M.A.A. Ibrahim, A.-S.S.M. Rady, P.A. Sidhom, S.R.M. Sayed, K.E. Ibrahim, A. M. Awad, T. Shoeib, L.A. Mohamed, A Comparative DFT Investigation of the Adsorption of Temozolomide Anticancer Drug over Beryllium Oxide and Boron Nitride Nanocarriers, ACS Omega 9 (2024) 25203–25214.
[69] A. Maleki, Adsorption behavior of anti-cancer procarbazine on the surface of on pristine, Al-, Si-, and C-doped B24N24 fullerenes based on the density functional theory, Struct. Chem. 33 (2022) 323–333.
[70] A. Maleki, S. Esmaielzadeh, S. Fakhraee, Performance of C60 fullerene, pristine, and Si/Al-doped B12N12 fullerenes as potential sensor for dacarbazine drug, Theor. Chem. Accounts 143 (2024) 39.
[71] S. Ketabi, S. Shalmashi, S. Hallajian, Interaction of sulfasalazine with outer surface of boron-nitride nanotube as a drug carrier in aqueous solution: insights from quantum mechanics and Monte Carlo simulation, BMC Chemistry 17 (2023) 169.
[72] A.J. Bin Iqbal, R. Shahriar, A. Zubair, First-principles study of a SiC nanosheet as an effective material for nitrosourea and carmustine anti-cancer drug delivery, Nanoscale Adv. 6 (2024) 2968–2979.
[73] Y. Zhang, Y. Luo, L. Tang, M. E, J. Hu, Unveiling regularities of B12N12-X nanocages as a drug delivery vehicle for the nitrosourea: the influence of periods and groups, J. Mol. Liq. 393 (2024) 123607.
[74] A. Hosseinian, A. Bekhradnia, E. Vessally, L. Edjlali, M.D. Esrafili, A theoretical study on the C30X15Y15 (X=B, and Al; Y=N, and P) heterofullerenes, Comput. Theor. Chem. 1115 (2017) 114–118.
[75] M.K. Hazrati, Z. Bagheri, A. Bodaghi, Application of C30B15N15 heterofullerene in the isoniazid drug delivery: DFT studies, Phys. E: Low-dimensional Syst. Nanostruct. 89 (2017) 72–76.
[76] X.F. Fan, Z. Zhu, Z.X. Shen, J.-L. Kuo, On the Use of Bond-Counting Rules in Predicting the Stability of C12B6N6 Fullerene, J. Phys. Chem. C 112 (2008) 15691–15696.
[77] İ. Muz, F. Göktaş, M. Kurban, A density functional theory study on favipiravir drug interaction with BN-doped C60 heterofullerene, Phys. E Low-Dimens. Syst. Nanostruct. 135 (2022) 114950.
[78] D. Paul, J. Deb, B. Bhattacharya, U. Sarkar, Electronic and optical properties of C 24, C 12 X 6 Y 6, and X 12 Y 12 (X= B, Al and Y= N, P), J. Mol. Model. 24 (2018) 1–13.
[79] M. Anafcheh, R. Ghafouri, F. Naderi, Exploring electronic structures for the most stable isomers of C12B6N6 and B6N6C12 heterofullerenes based on NMR, NICS and NBO analysis: a DFT study, Phys. E Low-Dimens. Syst. Nanostruct. 44 (2012) 1992–1998.
[80] C.A. Celaya, L.F. Hernández-Ayala, F. Buendía Zamudio, J.A. Vargas, M. Reina, Adsorption of melphalan anticancer drug on C24, B12N12, B12C6N6, B6C12N12 and B6C6N12 nanocages: A comparative DFT study, J. Mol. Liq. 329 (2021) 115528.
[81] M.J. Frisch, G.W. Trucks, H.B. Schlegel, G.E. Scuseria, M.A. Robb, J. R. Cheeseman, G. Scalmani, V. Barone, G.A. Petersson, H. Nakatsuji, X. Li, M. Caricato, A.V. Marenich, J. Bloino, B.G. Janesko, R. Gomperts, B. Mennucci, H. P. Hratchian, J.V. Ortiz, A.F. Izmaylov, J.L. Sonnenberg, Williams, F. Ding, F. Lipparini, F. Egidi, J. Goings, B. Peng, A. Petrone, T. Henderson, D. Ranasinghe, V.G. Zakrzewski, J. Gao, N. Rega, G. Zheng, W. Liang, M. Hada, M. Ehara, K. Toyota, R. Fukuda, J. Hasegawa, M. Ishida, T. Nakajima, Y. Honda, O. Kitao, H. Nakai, T. Vreven, K. Throssell, J.A. Montgomery Jr., J.E. Peralta, F. Ogliaro, M. J. Bearpark, J.J. Heyd, E.N. Brothers, K.N. Kudin, V.N. Staroverov, T.A. Keith, R. Kobayashi, J. Normand, K. Raghavachari, A.P. Rendell, J.C. Burant, S. S. Iyengar, J. Tomasi, M. Cossi, J.M. Millam, M. Klene, C. Adamo, R. Cammi, J. W. Ochterski, R.L. Martin, K. Morokuma, O. Farkas, J.B. Foresman, D.J. Fox, Wallingford, CT, 2016.
[82] A.D. Becke, Density-functional thermochemistry. III. The role of exact exchange, J. Chem. Phys. 98 (1993) 5648–5652.
[83] A.D. Becke, A new mixing of Hartree–Fock and local density-functional theories, J. Chem. Phys. 98 (1993) 1372–1377.
[84] M.D. Mohammadi, H.Y. Abdullah, G. Biskos, S. Bhowmick, Enhancing the absorption of 1-chloro-1,2,2,2-tetrafluoroethane on carbon nanotubes: an ab initio study, Bull. Mater. Sci. 44 (2021) 198.
[85] J. Tomasi, B. Mennucci, R. Cammi, Quantum Mechanical Continuum Solvation Models, Chem. Rev. 105 (2005) 2999–3094.
[86] J.P. Merrick, D. Moran, L. Radom, An evaluation of harmonic vibrational frequency scale factors, J. Phys. Chem. A 111 (2007) 11683–11700.
[87] S.A. Bithe, M. Hasan, A.A. Oishi, P. Dhali, D. Roy, To understand the miglitol adsorption behavior on BC3, BN, and GNS nanosheets using DFT and QTAIM analysis for drug delivery applications, Phys Scr 98 (2023) 075010.
[88] M. Akhondi, E. Jamalizadeh, A. Mohebbi, MD and DFT calculations on the structural variations of amino-cyclodextrin as a pH-sensitive carrier for smart carriage and release of Doxorubicin, J. Mol. Struct. 1230 (2021) 129855.
[89] N.M. O'boyle, A.L. Tenderholt, K.M. Langner, Cclib: a library for package-independent computational chemistry algorithms, J. Comput. Chem. 29 (2008) 839–845.
[90] W. Humphrey, A. Dalke, K. Schulten, VMD: visual molecular dynamics, J. Mol. Graph. 14 (1996) 33–38.
[91] T. Lu, F. Chen, Multiwfn: A multifunctional wavefunction analyzer, J. Comput. Chem. 33 (2012) 580–592.
[92] L. Fallon, III, The crystal and molecular structure of 5-fluorouracil, Acta Cryst. Sect. B Struct. Sci. Cryst. Eng. Mater. 29 (1973) 2549–2556.
[93] B. Blicharska, T. Kupka, Theoretical DFT and experimental NMR studies on uracil and 5-fluorouracil, J. Mol. Struct. 613 (2002) 153–166.
[94] M. Sadeghi, B. Khoshnevisan, DFT study of Ti3C2 MXene nanosheets as a drug delivery system for 5-fluorouracil, RSC Adv. 14 (2024) 20300–20311.
[95] G.J. Ogunwale, H. Louis, T.O. Unimuke, G.E. Mathias, A.E. Owen, H.O. Edet, O. C. Enudi, E.O. Oluwasanmi, A.S. Adeyinka, M. Doust Mohammadi, Interaction of 5-Fluorouracil on the surfaces of pristine and functionalized Ca12O12 nanocages: an intuition from DFT, ACS Omega 8 (2023) 13551–13568.
[96] L. Zhang, Z.D. Qi, Y.L. Ye, X.H. Li, J.H. Chen, W.M. Sun, DFT study on the adsorption of 5-fluorouracil on B(40), B(39)M, and M@B(40) (M = Mg, Al, Si, Mn, Cu, Zn), RSC Adv. 11 (2021) 39508–39517.
[97] M.H. Miah, M.R. Hossain, M.S. Islam, T. Ferdous, F. Ahmed, A theoretical study of allopurinol drug sensing by carbon and boron nitride nanostructures: DFT, QTAIM, RDG, NBO and PCM insights, RSC Adv. 11 (2021) 38457–38472.
[98] A. Escobedo-Morales, L. Tepech-Carrillo, A. Bautista-Hernández, J.H. Camacho-García, D. Cortes-Arriagada, E. Chigo-Anota, Effect of Chemical Order in the Structural Stability and Physicochemical Properties of B12N12 Fullerenes, Sci. Rep. 9 (2019) 16521.
[99] A. Soltani, E. Tazikeh-Lemeski, M.B. Javan, A comparative theoretical study on the interaction of pure and carbon atom substituted boron nitride fullerenes with ifosfamide drug, J. Mol. Liq. 297 (2020) 111894.
[100] D. Paul, J. Deb, B. Bhattacharya, U. Sarkar, Electronic and optical properties of C24, C12X6Y6, and X12Y12 (X=B, Al and Y=N, P), J. Mol. Model. 24 (2018) 204.
[101] F. Li, Y. Zhang, H. Chen, Geometric and electronic structures of B12C6N6 fullerene, Phys. E: Low-dimensional Syst. Nanostruct. 56 (2014) 216–221.
[102] M.B. Javan, A. Soltani, Z. Azmoodeh, N. Abdolahi, N. Gholami, A DFT study on the interaction between 5-fluorouracil and B12N12 nanocluster, RSC Adv. 6 (2016) 104513–104521.
[103] N. Wazzan, K.A. Soliman, W.S.A. Halim, Theoretical study of gallium nitride nanocage as a carrier for 5-fluorouracil anticancer drug, J. Mol. Model. 25 (2019) 265.
[104] S.F. Boys, F. Bernardi, The calculation of small molecular interactions by the differences of separate total energies. Some procedures with reduced errors, Mol. Phys. 19 (1970) 553–566.
[105] M.R. Hossain, M.M. Hasan, M. Nishat, E.A. Noor, F. Ahmed, T. Ferdous, M. A. Hossain, DFT and QTAIM investigations of the adsorption of chlormethine anticancer drug on the exterior surface of pristine and transition metal functionalized boron nitride fullerene, J. Mol. Liq. 323 (2021) 114627.
[106] I. Benjamin, H. Louis, G.A. Okon, S.W. Qader, L.E. Afahanam, C.F. Fidelis, E. A. Eno, E.E. Ejiofor, A.-L.E. Manicum, Transition Metal-Decorated B12N12–X (X = Au, Cu, Ni, Os, Pt, and Zn) Nanoclusters as Biosensors for Carboplatin, ACS Omega 8 (2023) 10006–10021.
[107] R. Sainda, D. Chodvadiya, P.K. Jha, A DFT study of Mg9O9 nanoring for gas sensing and removal applications, J. Mol. Liq. 397 (2024) 124121.

[108] D. Chodvadiya, J. Panchal, I. Zgłobicka, K.J. Kurzydłowski, P.K. Jha, A density functional theory study on the prediction of stable Be9O9 nanoring and its application as an atmospheric gas (CO, NO and NH3) sensor, Mater. Sci. Semicond. Process. 196 (2025) 109672.
[109] M. Kamel, H. Raissi, A. Morsali, M. Shahabi, Assessment of the adsorption mechanism of Flutamide anticancer drug on the functionalized single-walled carbon nanotube surface as a drug delivery vehicle: An alternative theoretical approach based on DFT and MD, Appl. Surf. Sci. 434 (2018) 492–503.
[110] E.R. Johnson, S. Keinan, P. Mori-Sánchez, J. Contreras-García, A.J. Cohen, W. Yang, Revealing Noncovalent Interactions, J. Am. Chem. Soc. 132 (2010) 6498–6506.
[111] S. Thomas, M. Asle Zaeem, Phosgene gas sensing of Ti2CT2 (T = F−, O−, OH−) MXenes, Adv. Theory Simul. 4 (2021) 2000250.
[112] S. Thomas, V. Kumar, D.R. Roy, M.A. Zaeem, Two-dimensional boron–phosphorus monolayer for reversible NO2 gas sensing, ACS Appl. Nano Mater. 3 (2020) 10073–10081.
[113] H.O. Muhsen, A.O.M. Almayyali, A.Y. Al-Mamoori, F.F. Mahmood, Theoretical analysis of the structural and electronic properties of the interaction of boron nitride diamantane nanocrystal with the drug hydroxyurea as an anticancer drug, J. Mol. Model. 27 (2021) 90.
[114] J.S. Al-Otaibi, Y.S. Mary, Y.S. Mary, S. Kaya, G. Serdaroglu, DFT computational study of trihalogenated aniline derivative's adsorption onto graphene/fullerene/fullerene-like nanocages, X12Y12 (X = Al, B, and Y = N, P), J. Biomol. Struct. Dyn. 40 (2022) 8630–8643.
[115] J.S. Al-Otaibi, Y.S. Mary, Y.S. Mary, N. Acharjee, D.G. Churchill, Spectroscopic studies of 5-fluoro-1H-pyrimidine-2,4-dione adsorption on nanorings, solvent effects and SERS analysis, Comput. Theor. Chem. 1217 (2022) 113873.
[116] Z. Ullah, B. Mustafa, H.J. Kim, Y. Sheena Mary, Y. Shyma Mary, H.W. Kwon, DFT of 5-Fluoro-2-Oxo-1H-Pyrazine-3-Carboxamide (OPC) Adsorption, Spectroscopic, Solvent Effect, and SERS Analysis, J. Mol. Liq. 357 (2022) 119076.